ARTICLE

Cadmium activates AMPA and NMDA receptors with M3 helix cysteine substitutions

Timothy J. Wilding and James E. Huettner

AMPA and NMDA receptors are ligand-gated ion channels that depolarize postsynaptic neurons when activated by the neurotransmitter L-glutamate. Changes in the distribution and activity of these receptors underlie learning and memory, but excessive change is associated with an array of neurological disorders, including cognitive impairment, developmental delay, and epilepsy. All of the ionotropic glutamate receptors (iGluRs) exhibit similar tetrameric architecture, transmembrane topology, and basic framework for activation; conformational changes induced by extracellular agonist binding deform and splay open the inner helix bundle crossing that occludes ion flux through the channel. NMDA receptors require agonist binding to all four subunits, whereas AMPA and closely related kainate receptors can open with less than complete occupancy. In addition to conventional activation by agonist binding, we recently identified two locations along the inner helix of the GluK2 kainate receptor subunit where cysteine (Cys) substitution yields channels that are opened by exposure to cadmium ions, independent of agonist site occupancy. Here, we generate AMPA and NMDA receptor subunits with homologous Cys substitutions and demonstrate similar activation of the mutant receptors by Cd. Coexpression of the auxiliary subunit stargazin enhanced Cd potency for activation of Cys-substituted GluA1 and altered occlusion upon treatment with sulfhydryl-reactive MTS reagents. Mutant NMDA receptors displayed voltage-dependent Mg block of currents activated by agonist and/or Cd as well as asymmetry between Cd effects on Cys-substituted GluN1 versus GluN2 subunits. In addition, Cd activation of each Cys-substituted iGluR was inhibited by protons. These results, together with our earlier work on GluK2, reveal a novel mechanism shared among the three different iGluR subtypes for prying open the gate that controls ion entry into the pore.

Introduction

Ionotropic glutamate receptors (iGluRs) are gated pores through the plasma membrane that mediate neurotransmission at excitatory synapses in the central nervous system (Traynelis et al., 2010). Each receptor is a modular tetramer with extracellular amino-terminal and ligand-binding domains (ATD and LBD, respectively), a pore-forming transmembrane domain (TMD), and a cytoplasmic carboxy-terminal domain involved with trafficking and regulation by intracellular proteins (Traynelis et al., 2010). The three main iGluR subtypes named for the agonists kainate, α-amino-3-hydroxy-5-methyl-4-isoxazole-propionate (AMPA), and NMDA comprise separate sets of subunits that exhibit similar transmembrane topology despite limited primary sequence identity (Traynelis et al., 2010). In addition to their essential role in normal physiology, increasing evidence highlights the detrimental consequences of aberrant iGluR activation resulting from elevated extracellular glutamate (Bano and Ankarcrona, 2018), de novo point mutations (Guzmán et al., 2017; Fernández-Marmiesse et al., 2018; Fry et al., 2018; Li et al., 2016), or autoimmune modulation of receptor activity (Gleichman et al., 2012).

Indeed, recent work to understand iGluR operation and identify subtype-selective antagonists and allosteric modulators has been fueled by the growing list of neuropathologies attributed to acute or chronic iGluR hypo- or hyperactivation.

Much of the work on iGluR gating and permeation has focused on the TMD, which resembles an inverted potassium channel (Kuner et al., 2003; Huettner 2015). Each of the four subunits contributes a pore loop (M2) including a short helix and open coil that dips into the plane of the membrane from the cytoplasmic side and is flanked by inner (M3) and outer (M1) transmembrane helices (Sobolevsky et al., 2009). All eukaryotic iGluRs possess an additional transmembrane helix (M4) that contacts M1 and M3 of the adjacent subunit (Terhag et al., 2010; Salussolia et al., 2013). The gate for ion flux through the pore is formed by a tight occlusion at the bundle crossing of the inner (M3) helices (Twomey and Sobolevsky, 2018), which include a conserved 9-amino acid (SYTANLAAF) motif in all of the iGluR subunits (Kuner et al., 2003). Agonist binding to the extracellular LBD opens iGluR channels by pulling on short linkers that distort

Department of Cell Biology and Physiology, Washington University Medical School, St. Louis, MO.

Correspondence to James E. Huettner: jhuettner@wustl.edu.
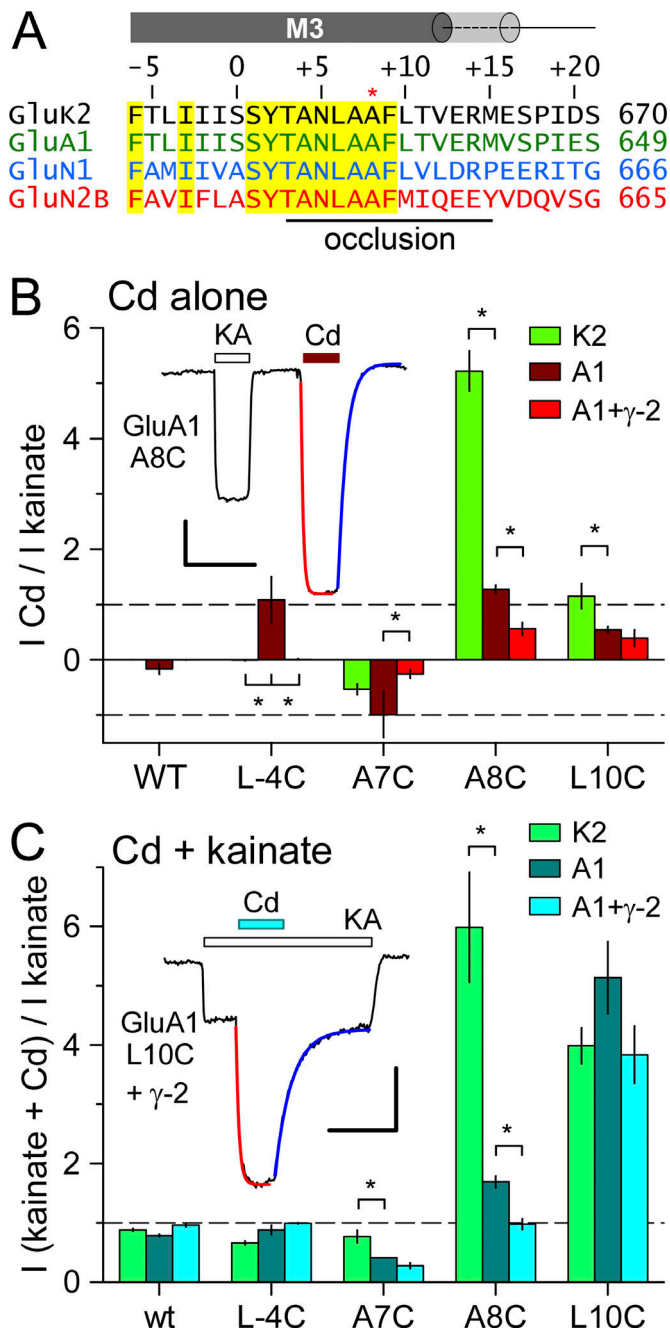
Figure 1. **AMPA receptor activation by Cd. (A)** iGluR subunit sequence alignment near the M3 helix bundle-crossing occlusion. Numbers on the right indicate position of the final residue from the amino terminal methionine. Homologous positions are numbered above the sequences relative to the first conserved residue in the SYTANLAAF motif. Yellow highlights sequence identity. The A8 Lurcher site is marked with an asterisk. In the AMPA receptor closed state, the M3 helix extends to approximately +17 and +12 in the A/C and B/D conformations, respectively, as depicted by gray cylinders above the sequence. **(B and C)** Current evoked by 50 µM Cd alone (B) or together with kainate (C) as a fraction of current evoked by kainate alone (mean ± SEM, 6–33 cells per AMPA receptor construct). Data for GluK2 were derived from Wilding and Huettner (2019). Asterisks denote significant difference from GluA1 (one-way ANOVA with post hoc Dunn's comparison to control). Insets show whole-cell currents evoked by 100 µM kainate (KA, open bar) and 50 µM Cd alone (red bar) for homomeric GluA1 A8C (B) or by 50 µM Cd together with kainate (cyan bar) for GluA1 L10C + stargazin (C). Single exponential fits to the onset (red line) and recovery (blue line) of Cd responses are shown in B (τ_{on} = 540 ms; τ_{off} = 3.6 s) and C (τ_{on} = 2.0 s; τ_{off} = 7.5 s). Scale bars represent 30 s and 100 pA (B) or 400 pA (C).

the M3 helices at the bundle crossing (Chen et al., 2017; Twomey et al., 2017), disrupting the occlusion zone to allow ions and water into the central cavity. Despite this common framework, NMDA and non-NMDA (AMPA/kainate) receptors exhibit significant differences in their gating and permeation properties. For example, activation of AMPA (Rosenmund et al., 1998; Smith and Howe, 2000) and kainate (Swanson et al., 2002; Fisher and Mott, 2011) receptors does not require agonist binding to all four subunits, whereas conventional diheteromeric NMDA receptors remain closed unless all four subunit LBDs are occupied (Johnson and Ascher, 1987; Kleckner and Dingledine, 1988), with glutamate binding to the GluN2 subunits and glycine or D-serine binding to GluN1 (Traynelis et al., 2010).

In addition to physiological gating by agonist binding to the LBD, we recently identified mutations in the M3 helix of the GluK2 kainate receptor subunit that allow channels to be opened by cadmium applied in the absence of LBD agonists (Wilding and Huettner, 2019). Exposure to Cd produces rapid and reversible activation of receptors that include subunits with Ala to Cys substitution at position 8 in the SYTANLAAF motif (S = 1) or with Leu to Cys substitution at position 10 immediately following this motif (see Fig. 1 A). Here we analyze the effect of Cd exposure on AMPA and NMDA receptors with homologous Cys substitutions. Our results demonstrate activation by Cd in the absence of added agonist and/or potentiation of agonist-evoked current by Cd coapplication for both Cys substitutions. As we found for GluK2 kainate receptors (Wilding and Huettner, 2019), Cd exhibits higher potency at AMPA and NMDA receptors with the A8C than the L10C substitution. In addition, recordings from heteromeric receptors confirmed that A8C or L10C replacement is not required on all four subunits within the tetramer. Together, this work identifies a novel mechanism shared among the three iGluR subtypes for prying open the bundle-crossing gate (Wollmuth, 2019).

Materials and methods

cDNA constructs, cell culture, and transfection

Plasmids with DNA encoding WT AMPA and NMDA receptor channels were generously provided by Drs. Steve Heinemann (Salk Institute, La Jolla, CA), Peter Seeburg (Max Planck Institute, Heidelberg, Germany), Doris Patneau (Oklahoma State University, Stillwater, OK), and Stefano Vicini (Georgetown University, Washington, D.C.). Point mutations were generated with the QuikChange XL system (Agilent) or by PCR (Lopez et al., 2013). All constructs were verified by DNA sequencing. HEK293 cells at 50–70% confluence were transfected with 1–3 µg plasmid DNA using lipofectamine 2000 (ThermoFisher). Coexpression of a plasmid encoding GFP was used to identify transfected cells. One day after transfection, cells were dissociated with protease and replated at low density on nitrocellulose-treated 35-mm dishes (Wilding et al., 2008). Recordings were obtained from green fluorescent cells 24–48 h after replating.

Electrophysiology

Whole-cell recordings were obtained on an inverted microscope equipped with epifluorescent illumination. The culture dish was perfused with Tyrode's solution (in mM): 150 NaCl, 4 KCl,

2 CaCl$_2$, 2 MgCl$_2$, 10 glucose, and 10 HEPES, pH adjusted to 7.4 with NaOH. Borosilicate electrodes had an open tip resistance of 2–5 MOhm when filled with internal solution (in mM): 140 Cs-glucuronate, 10 EGTA, 5 CsCl, 5 MgCl$_2$, 5 ATP, 1 GTP, and 10 HEPES buffer, pH adjusted to 7.4 with CsOH. Agonists and/or Cd were dissolved in 160 mM NaCl, 2 mM CaCl$_2$ and 10 mM HEPES (pH 7.4 with NaOH) and applied by local perfusion from an 8-barrelled gravity-driven capillary pipette (Wilding et al., 2005). Currents were recorded with an Axopatch 200A amplifier (Molecular Devices) controlled by pClamp software.

Analysis

Current–voltage relations were generated and analyzed from triangle wave ramps as described (Lopez et al., 2013). For concentration–inhibition experiments, current recorded during exposure to agonist plus Cd was plotted as a fraction of control current evoked by agonist alone. Concentration–inhibition results were fit with the following equation: I/I control = 1 / [1 + ([Cd] / IC$_{50}$)^b], where IC$_{50}$ is the Cd concentration producing half-maximal inhibition and b is the slope factor or Hill coefficient. Steady-state currents evoked by Cd were normalized to the maximal Cd response (I max) and fit with the following equation: I/I max = {1 / [1 + (EC$_{50}$ / [Cd])^n]} / [1 + ([Cd] / IC$_{50}$)^b], where EC$_{50}$ and IC$_{50}$ are the Cd concentrations producing half-maximal activation and inhibition, respectively, and n and b are the slope factors for activation and inhibition. In some cases, an additional scaling factor was used to reflect the fact that steady-state current never achieved the maximal level (I max) recorded during the initial peak or tail response.

Results are reported as mean ± SEM, and significance was assigned for P < 0.05. One-way and two-way ANOVA and t tests were performed with SigmaStat (Systat Software). Curve fits using different numbers of parameters were evaluated by the ratio of residual variance test, F-statistic (Swartz et al., 1992).

Online supplemental material

Fig. S1 shows activation by kainate and inhibition by Cd of whole-cell currents in HEK293 cells transfected with A7C substituted GluK2(Q) and GluA1. Fig. S2 compares activation by kainate or by glutamate plus cyclothiazide for GluA1 WT, A8C, or L10C with or without γ-2 transmembrane AMPA receptor regulatory protein (TARP) coexpression. Fig. S3 shows activation by Cd compared with glutamate for A8C or L10C mutant GluA1 expressed alone or together with γ-2 TARP. Fig. S4 shows current–voltage relations for agonist and Cd activated currents mediated by GluA1 A8C and L10C. Fig. S5 shows Mg block of NMDA receptors with L10C substitutions. Fig. S6 shows proton inhibition of Cys-substituted non-NMDA receptor Cd activation.

Results

Cd activates AMPA receptors with M3 helix cysteine (Cys) substitutions

GluK2 kainate receptors with Cys substitutions at the A8 and L10 position in the M3 helix occlusion zone (Fig. 1 A) can be directly activated by exposure to Cd in the absence of agonist (Wilding and Huettner, 2019). To determine whether this is a feature unique to GluK2 or a general property shared among iGluR subunits, we first analyzed the effect of 50 µM Cd on homomeric GluA1 AMPA receptors with homologous A8C or L10C substitutions (Fig. 1, B and C). In addition, we tested two other GluA1 M3 helix Cys substitutions (L-4C and A7C) that were shown to be sensitive to Cd coapplication with agonist in previous work on homomeric GluA1 receptors expressed in *Xenopus laevis* oocytes (Sobolevsky et al., 2004). For the experiments in Fig. 1, we expressed WT or mutant GluA1 subunits in HEK293 cells alone or together with the γ-2 TARP, an auxiliary subunit that is also known as stargazin (Greger et al., 2017). In cells that received WT GluA1 50 µM Cd caused minimal change in the holding current when applied alone at −80 mV and had little effect on agonist-evoked current during coapplication with 100 µM kainate (Fig. 1, B and C). In contrast, Cd alone reduced the constitutive holding current recorded in cells expressing homomeric A7C mutant receptors (Fig. S1) and directly activated current in cells transfected with either the A8C or L10C mutations. In addition, coapplication of Cd with kainate revealed stronger inhibition than WT GluA1 for receptors with the A7C substitution but substantial potentiation for GluA1 bearing the L10C mutation. In most cells, the onset and recovery of Cd-evoked responses were well described by single exponential functions, although some cells exhibited a second slower kinetic component that may reflect tighter Cd coordination (Fig. 1, B and C, insets). When compared with homomeric mutant GluK2 kainate receptors (Wilding and Huettner, 2019), 50 µM Cd coapplication with agonist produced stronger inhibition of agonist-evoked current for the A7C mutant of GluA1 than for GluK2, similar potentiation for L10C substitution of GluA1 or GluK2, but weaker potentiation for the A8C mutation of GluA1 versus GluK2 (Fig. 1 C). Together, these results show that A8C or L10C substitution renders both AMPA and kainate receptors sensitive to activation by Cd.

Coexpression of γ-2 TARP tended to reduce the action of Cd relative to agonist alone. For example, Cd potentiated kainate-evoked current ~1.5-fold for GluA1 A8C expressed alone but had no significant effect with stargazin coexpression. Because γ-2 TARP can enhance the efficacy of partial agonists, such as kainate, for activation of WT receptors (Tomita et al., 2005; Turetsky et al., 2005), we also tested for this effect on homomeric A8C or L10C mutant GluA1. Experiments summarized in Fig. S2 confirmed the increase in kainate efficacy for WT GluA1 but revealed no difference in kainate relative to glutamate for either the A8C or L10C mutants with γ-2 TARP coexpression (Fig. S2). In addition, the positive allosteric modulator cyclothiazide (Yamada and Tang, 1993) had almost no effect on steady-state currents evoked by glutamate at receptors with A8C substitution and caused weaker potentiation of receptors with L10C substitution than occurs for WT GluA1 (Fig. S2). As shown in Fig. S3 we also compared currents evoked by Cd and glutamate. Co-transfection with γ-2 TARP had no effect on direct activation of GluA1 A8C or L10C by Cd alone (Fig. S3), but reduced activation of both mutants by coapplication of Cd and glutamate (Fig. S3) or of the L10C mutant by cyclothiazide and glutamate (Fig. S2). Thus, agonist-gated currents mediated by receptors with A8C or L10C substitutions exhibit less positive

allosteric modulation by Cd or cyclothiazide when γ-2 TARP is coexpressed.

Concentration dependence of Cd activation and inhibition

Before evaluating the concentration dependence of Cd activation at mutant receptors, we tested WT receptors with higher Cd concentrations. As shown in Fig. 2, half-maximal inhibition of kainate-evoked current mediated by WT GluA1 subunits expressed alone or together with γ-2 TARP required millimolar Cd (see Mayer et al., 1989). Individual inhibition curve fits illustrated in Fig. 2 B yielded IC_{50} estimates of 1.1 ± 0.3 and 2.9 ± 1.3 mM or GluA1 alone and GluA1 plus γ-2 TARP, respectively, but were not statistically superior to a simultaneous fit with a single curve ($IC_{50} = 2.1 \pm 0.6$ mM, $b = 0.75 \pm 0.15$; $P > 0.05$, F-statistic). Thus, millimolar concentrations of Cd inhibit homomeric WT GluA1 AMPA receptors and TARP coexpression has minimal effect on the potency of Cd inhibition.
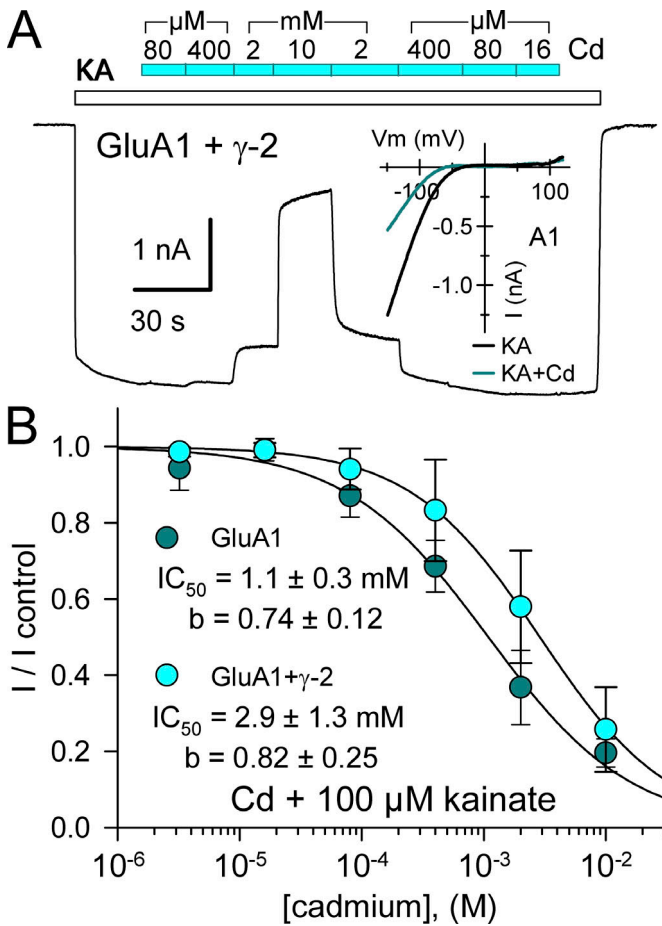
In contrast to WT GluA1, homomeric receptors formed by GluA1 A8C displayed monotonic activation and recovery with exposure to low Cd concentrations (<50 μM), whereas 400 μM and 2 mM Cd elicited multiphasic currents with an initial peak followed by decay to a lower steady-state plateau and prominent tail current on Cd washout (Fig. 3 A). As for kainate receptor A8C and L10C mutations (Wilding and Huettner, 2019), we interpret these multiphasic currents as a composite response that includes low-affinity inhibition superimposed on higher affinity current activation. Potency of activation by Cd alone was similar for A8C mutant AMPA and kainate receptors, with half-maximal values of 4.8 ± 1 μM for GluA1 A8C (Fig. 3 B) and 7.3 ± 1.4 μM for GluK2 A8C (Wilding and Huettner, 2019), respectively. In contrast, the IC_{50} of 360 ± 80 μM for steady-state Cd-evoked current (Fig. 3 B) revealed greater potency for inhibition of GluA1 A8C compared with inhibition of WT GluA1 by millimolar Cd (Fig. 2 B) or of GluK2 A8C, which requires >10 mM Cd for steady-state half-maximal inhibition (Wilding and Huettner, 2019). We
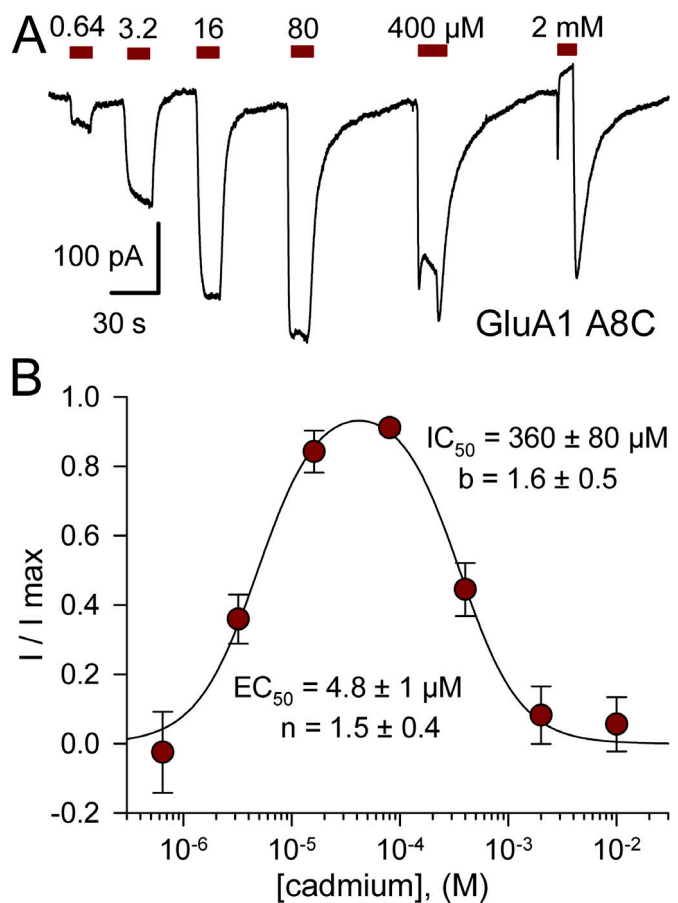

Figure 2. **Cd inhibits WT GluA1. (A)** Whole-cell current evoked by 100 μM kainate (open bar) in an HEK293 cell cotransfected with GluA1 and stargazin. The cyan bar indicates periods of Cd coapplication at 0.016, 0.08, 0.4, 2, or 10 mM. Inset shows the current–voltage relations for kainate alone or with 2 mM Cd in a cell transfected with GluA1. **(B)** Current recorded during Cd coapplication plotted as a fraction of control current immediately before or after Cd exposure (mean ± SEM; five cells for GluA1 alone, eight cells for GluA1 plus γ-2 TARP). Smooth curves are best fit of I/I control = $1 / [1 + ([Cd] / IC_{50})^b]$, where IC_{50} is the Cd concentration that produced half-maximal inhibition and b is the slope factor.

Figure 3. **Concentration dependence of GluA1 A8C activation and inhibition. (A)** Whole-cell currents evoked by increasing concentrations of Cd from 640 nM to 2 mM in an HEK293 cell transfected with GluA1 A8C. **(B)** Steady-state current recoded during exposure to each Cd concentration as a fraction of the maximal Cd-evoked response (mean ± SEM; 12 cells). Smooth curve is the best fit of I/I max = $\{1 / [1 + (EC_{50} / [Cd])^n]\} / [1+([Cd]/IC_{50})^b]$, where EC_{50} and IC_{50} are the Cd concentrations producing half-maximal activation and inhibition, respectively; n and b are the slope factors for activation and inhibition.
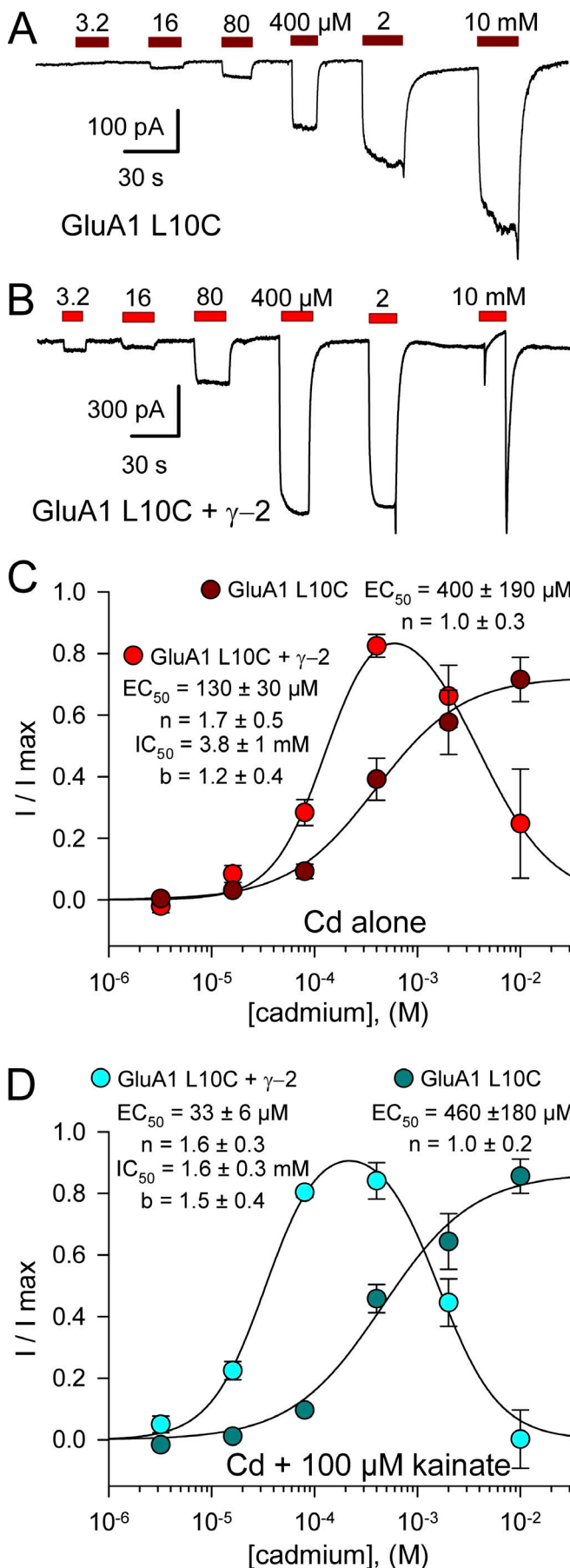
performed more extensive tests for concentration dependence of Cd action on the GluA1 L10C mutation, evaluating a range of doses for Cd alone as well as Cd together with a fixed concentration of 100 µM kainate on GluA1 L10C expressed alone or together with γ-2 TARP. Compared with GluA1 A8C (Fig. 3), Cd displayed lower potency for homomeric GluA1 with the L10C mutation (Fig. 4; see also Wilding and Huettner, 2019). For receptors expressed without the auxiliary subunit, values for half-maximal activation by Cd alone (Fig. 4 C, dark red circles) and for potentiation of coapplied 100 µM kainate (Fig. 4 D, dark cyan circles) were 400 ± 190 and 460 ± 180 µM, respectively, which were not statistically superior to a simultaneous fit with a single curve (EC_{50} = 420 ± 140 µM, n = 1.0 ± 0.2; P > 0.5, F-statistic). The micromolar potency for Cd activation of GluA1 A8C and GluK2 A8C indicates that Cd binding likely involves interaction with at least two coordination groups (Puljung and Zagotta, 2011). In contrast, the weaker potency for activation of L10C mutant receptors suggests that multiple coordination sites are not required for Cd interaction with GluA1 L10C (Fig. 4) or GluK2 L10C (Wilding and Huettner, 2019), at least when these subunits are expressed alone.

Coexpression of γ-2 TARP with GluA1 L10C enhanced potency for Cd activation and enabled inhibition of steady-state current at higher Cd concentrations (Fig. 4). Half-maximal activation and inhibition for Cd alone (Fig. 4 C, bright red circles) required 130 ± 30 µM and 3.8 ± 1 mM Cd, respectively, whereas coapplication with 100 µM kainate (Fig. 4 D, bright cyan circles) yielded significantly lower half-maximal values of 33 ± 6 µM for the rising phase of Cd potentiation (P < 0.0001, t test) and 1.6 ± 0.3 mM for the decline in steady-state potentiation at higher Cd doses (P = 0.02, t test). These results, together with the data in Fig. 1, B and C, where effects of a fixed dose of Cd were plotted as a fraction of agonist-evoked current, suggest that coapplication with agonist increases Cd efficacy at GluA1 L10C, whereas coexpression of γ-2 TARP increases Cd potency and agonist coapplication only enhances Cd potency when γ-2 TARP is coexpressed.

Figure 4. **Concentration dependence of GluA1 L10C activation and inhibition. (A and B)** Whole-cell currents evoked by 3.2 µM to 10 mM Cd in HEK293 cells transfected with GluA1 L10C alone (A) or together with γ-2 TARP (B). **(C and D)** Steady-state Cd-evoked current relative to control for Cd alone (C) or relative to kainate alone for Cd plus kainate applications (D), plotted as a fraction of the maximal Cd-evoked response (mean ± SEM). Smooth curves are the best fits of I/I max = m / [1 + (EC_{50} / [Cd])^n] for GluA1 L10C alone or I/I max = {1 / [1+(EC_{50}/[Cd])^n]} / [1+([Cd]/IC_{50})^b] for GluA1 L10C plus γ-2 TARP, where EC_{50} and IC_{50} are the Cd concentrations producing half-maximal activation and inhibition, respectively; n and b are the slope factors for activation and inhibition; m is a scaling factor steady-state current less than the maximal response. For GluA1 L10C expressed alone, Cd activated current with an EC_{50} of 400 ± 190 µM (n = 1.0 ± 0.3, six cells) when applied alone (C, dark red circles) or 460 ± 180 µM (n = 1.0 ± 0.2, three cells) when applied with 100 µM kainate (D, dark cyan circles). Cells cotransfected with GluA1 L10C and γ-2 TARP were inhibited by high Cd concentrations and activated by lower concentrations. For Cd alone (C, bright red circles, 10 cells), EC_{50} = 130 ± 30 µM (n = 1.7 ± 0.5) and IC_{50} = 3.8 ± 1 mM (b = 1.2 ± 0.4). For Cd plus kainate (D, bright cyan circles, four cells), EC_{50} = 33 ± 6 µM (n = 1.6 ± 0.3) and IC_{50} = 1.6 ± 0.3 mM (b = 1.5 ± 0.4).
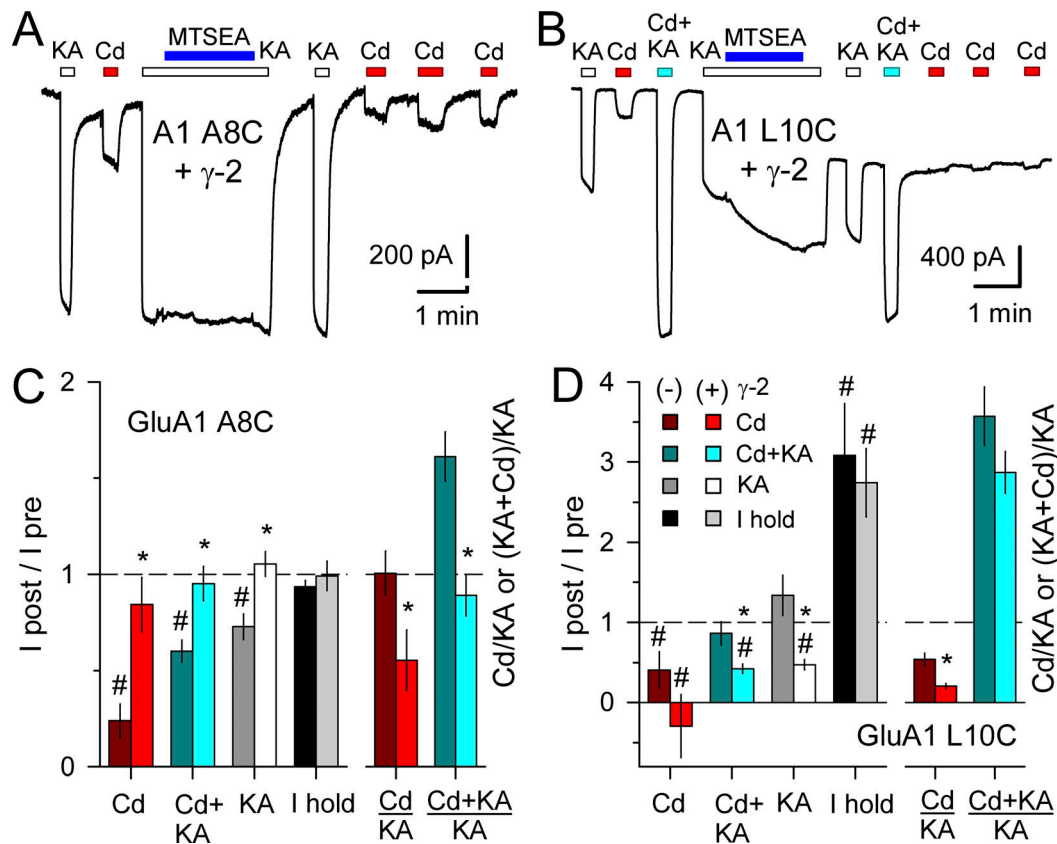
Figure 5. **MTSEA reduces Cd activation of GluA1 A8C and L10C. (A and B)** Whole-cell currents evoked by 100 µM kainate (open bars) or 50 µM Cd alone (red bars) or together with kainate (cyan bars) in HEK293 cells transfected with GluA1 A8C (A) or L10C (B) together with γ-2 TARP. **(A and C)** For the A8C mutation, exposure to MTSEA (blue bars) together with kainate caused little change in holding current or kainate-evoked current but reduced subsequent activation by Cd; the effect of MTS treatment was weaker in cells coexpressing γ-2 TARP (mean ± SEM; 6–29 cells per treatment). **(B and D)** For the L10C substitution, MTS treatment had a stronger effect in cells cotransfected with γ-2 TARP and caused a significant increase in holding current (mean ± SEM; 6–11 cells per treatment). For comparison with Fig 1, B and C, the Cd alone/kainate alone and Cd plus kainate/kainate alone current ratios in these cells before MTSEA exposure are shown in C and D. Asterisks denote significant difference with γ-2 TARP coexpression (one-way ANOVA with post hoc Student–Newman–Keuls test). # indicates significant difference from (I after/I before) = 1.

Partial occlusion by MTS reagents

Our previous work on GluK2 A8C and L10C showed that activation by Cd was substantially reduced after exposure to 2-aminoethyl MTS (MTSEA; Wilding and Huettner, 2019), a sulfhydryl-reactive compound that covalently modifies free Cys residues. Earlier work on GluA1 A8C or L10C expressed in oocytes reported little change in glutamate-evoked current following exposure to MTSEA (Sobolevsky et al., 2003); however, to test whether Cd activation of GluA1 A8C or L10C was affected by Cys modification we evaluated currents before and after several minutes exposure to kainate plus 100 µM MTSEA (Fig. 5). Plots in Fig. 5, C and D summarize the effect of MTSEA exposure on activation by Cd alone or together with 100 kainate, on activation by kainate alone, and on the current required to hold cells at –80 mV. Both mutant GluA1 subunits were tested in isolation as well as together with coexpressed γ-2 TARP. For GluA1 A8C expressed alone, exposure to MTSEA had little effect on the holding current but reduced activation by Cd, kainate, or Cd plus kainate (Fig. 5 C). MTSEA was significantly less effective on GluA1 A8C coexpressed with γ-2 TARP (Fig. 5, A and C; P = 0.0001, two-way ANOVA), causing a slight reduction in current activated by Cd alone but no

significant change in current evoked by kainate alone or kainate together with Cd (I after/I before ∼1). In contrast to the A8C mutant, MTSEA had a larger negative effect on activation of GluA1 L10C coexpressed with γ-2 TARP than on GluA1 L10C alone (Fig. 5, B and D; P = 0.021, two-way ANOVA). In addition, cells expressing GluA1 L10C, with or without γ-2 TARP, displayed a significant increase in holding current following exposure to MTSEA (Fig. 5, B and D; P < 0.0001, two-way ANOVA), as we previously observed for the GluK2 L10C substitution (Wilding and Huettner, 2019). Together, these results indicate at least partial occlusion of Cd activation by MTS modification. Coexpression of γ-2 TARP suppressed this effect for GluA1 A8C but enhanced it for GluA1 L10C. Lack of complete occlusion may be owing to our use of a relatively low MTSEA concentration (100 µM) compared with previous work (Sobolevsky et al., 2003), whereas the reason we observe a greater effect on GluA1 L10C than previous reported in oocytes remains unclear.

Cd activates heteromeric AMPA receptors

Although homomeric iGluRs with one M3 mutation per subunit will have a total of four introduced cysteines per receptor, our

previous work showed that all four substitutions are not required for Cd activation of GluK2 A8C or L10C (Wilding and Huettner, 2019). To test whether AMPA receptors with fewer than four cysteines near the bundle crossing can be activated by Cd, we coexpressed mutant GluA1 A8C (Fig. 6) or L10C (Fig. 7) together with WT edited GluA2(R). For both mutations, Cd activated heteromeric receptors, albeit with lower potency than for homomeric receptors with Cys substitutions on all four subunits (compare Figs. 3 B and 6 B with Figs. 4 C and 7 D). Cells cotransfected with the Q/R site-edited GluA2(R) subunit lacked strong inward rectification (Fig. 7 B) observed for unedited homomeric WT GluA1 (Boulter et al., 1990; Verdoorn et al., 1991) as well as the A8C and L10C mutant subunits (Fig. S4). The ability of Cd to activate heteromeric combinations indicates that Cys substitution is not required on all four AMPA receptor subunits.

Cd activates NMDA receptors with A8C substitution

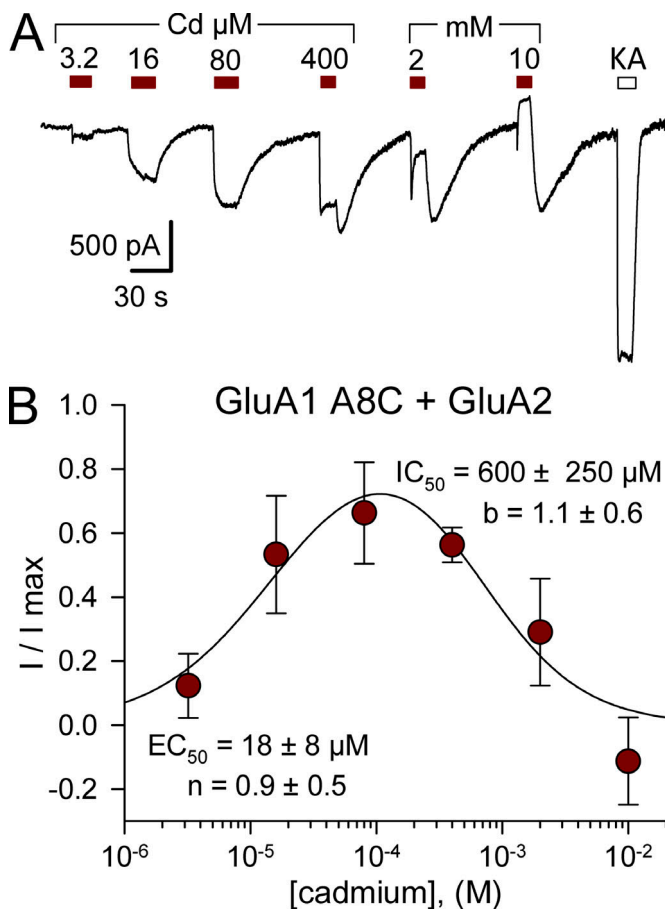NMDA receptors are obligate heteromers, requiring coexpression of the GluN1 subunit together with GluN2 and/or

Figure 6. Cd activates GluA1 A8C/GluA2 heteromeric receptors. (A) Whole-cell currents evoked by 3.2 µM to 10 mM Cd (red bars) or by 100 µM kainate (open bars) in HEK293 cells cotransfected with edited GluA2 and GluA1 A8C. **(B)** Steady-state Cd-evoked current plotted as a fraction of the maximal Cd-evoked response (mean ± SEM; five cells). Smooth curve is the best fits of $I/I_{max} = \{1 / [1 + (EC_{50} / [Cd])^n]\} / [1 + ([Cd] / IC_{50})^b]$, where EC_{50} and IC_{50} are the Cd concentrations producing half-maximal activation and inhibition, respectively; n and b are the slope factors for activation and inhibition.
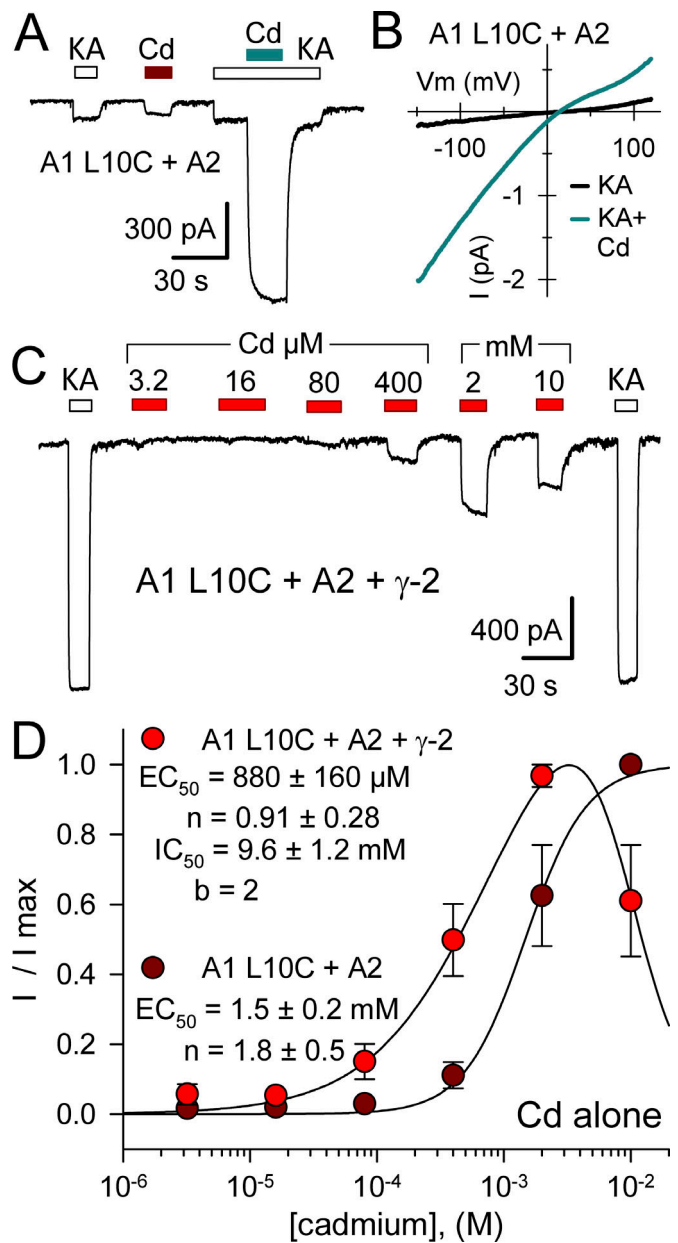

Figure 7. Cd activates GluA1 L10C/GluA2 heteromeric receptors. (A) Whole-cell currents evoked by 100 µM kainate (open bars) and 50 µM Cd alone (red bar) or together with kainate (cyan bar) in HEK293 cells cotransfected with edited GluA2 and GluA1 L10C. **(B)** Current evoked by 100 µM kainate (black line) or kainate plus 50 µM Cd (cyan line) during voltage ramps from −150 to +120 mV. **(C)** Whole-cell currents evoked by 3.2 µM to 10 mM Cd (red bars) or by 100 µM kainate (open bars) in HEK293 cells cotransfected with edited GluA2, GluA1 L10C, and γ-2 TARP. **(D)** Steady-state Cd-evoked current plotted as a fraction of the maximal Cd-evoked response (mean ± SEM; four cells with and five cells without γ-2 TARP). Smooth curves are the best fits of $I/I_{max} = 1 / [1 + (EC_{50} / [Cd])^n]$ for GluA1 L10C with GluA2 or $I/I_{max} = \{1 / [1 + (EC_{50} / [Cd])^n]\} / [1 + ([Cd] / IC_{50})^b]$ for GluA1 L10C with GluA2 and γ-2 TARP, where EC_{50} and IC_{50} are the Cd concentrations producing half-maximal activation and inhibition, respectively; n and b are the slope factors for activation and inhibition.

GluN3 subunits (Hansen et al., 2014; Pérez-Otaño et al., 2016). As an initial test for activation of M3 mutant NMDA receptors, we examined conventional diheteromeric channels formed by cotransfection of GluN1 and GluN2B subunits. For WT receptors,

exposure to 50 µM Cd alone caused negligible change in holding current, whereas coapplication with 10 µM NMDA and glycine produced modest block (~44.4%) of agonist-evoked current (Fig. 8, A and E; see also Mayer et al., 1989; Tu et al., 2016; Wilding and Huettner, 2019). In contrast, 50 µM Cd alone activated receptors with A8C substitution to GluN2B (Fig. 8, B and E), GluN1 (Fig. 8, C and E), or both subunits (Fig. 8, D and E), and coapplication of Cd potentiated current evoked by NMDA plus glycine (Fig. 8). As for AMPA (Fig. 3) and kainate (Wilding and Huettner, 2019) receptors, the A8C mutant NMDA receptors exhibited monotonic activation and decay for currents elicited by Cd concentrations <100 µM but increasing inhibition during steady-state exposure to higher Cd concentrations (Fig. 9 A). For cells cotransfected with both the N1 A8C and N2B A8C mutant subunits, current activation by Cd alone was half maximal at 24 ± 5 µM, whereas half-maximal steady-state inhibition required 1.5 ± 0.4 mM Cd (Fig. 9, A and B). Thus, A8C substitution to either two or all four of the subunits in a tetrameric channel enables activation by Cd for all three of the iGluR subtypes.

Subunit-dependent potentiation by Cd at the +10 position

To test for Cd activation of NMDA receptors with Cys substitutions at the +10 position, we generated GluN1 L10C and GluN2B M10C mutations and analyzed currents in cells transfected with N1 WT + N2B M10C, N1 L10C + N2B WT, or N1 L10C + N2B M10C (Fig. 10). In contrast to kainate (Wilding and Huettner, 2019) or AMPA (Figs. 1 and 4) receptors, Cd alone at 0.05, 0.5, and 5 mM failed to activate NMDA receptors with Cys substitutions at the +10 position of GluN1, GluN2B, or both subunits (Fig. 10 D). Moreover, coapplication of Cd together with 10 µM NMDA and glycine revealed striking differences among the subunit combinations. Exposure to Cd potentiated agonist-evoked currents mediated by mutant N1 L10C subunits combined with WT N2B (Fig. 10, B and E). In contrast, Cd strongly inhibited agonist-evoked current for receptors that included the N2B M10C subunit, combined with either WT N1 (Fig. 10, A and E) or N1 L10C (Fig. 10, C and E). Thus, for Cys substitution at the +10 position positive allosteric modulation by Cd is restricted to the N1 subunit, whereas Cd interaction with N2B M10C yields dominant inhibition over N1 WT or N1 L10C.

Mg block and potentiation

To test whether Cys substitution and/or interaction with Cd affects voltage-dependent channel block by Mg ions (Nowak et al., 1984; Mayer et al., 1984), we analyzed currents evoked by agonists and/or Cd in the presence and absence of 1 mM Mg (Fig. 11). Currents were evaluated during triangle wave voltage ramps from −150 to +120 mV (Fig. 11, A and B; Lopez et al., 2013), at steady-state holding potentials of −80 and +40 mV (Fig. 11 C), or with brief voltage steps from −80 mV to positive test potentials (Fig. 11 D). In cells transfected with WT receptor subunits, agonist-evoked currents were strongly blocked by Mg at negative potentials but slightly potentiated at positive potentials (Fig. 11, A and E), as previously reported (Paoletti et al., 1995) for the diheteromeric combination that we used (GluN2B plus the GluN1-1a splice variant that lacks extracellular exon 5; Hollmann et al., 1993). Currents evoked by NMDA and glycine, by Cd alone,
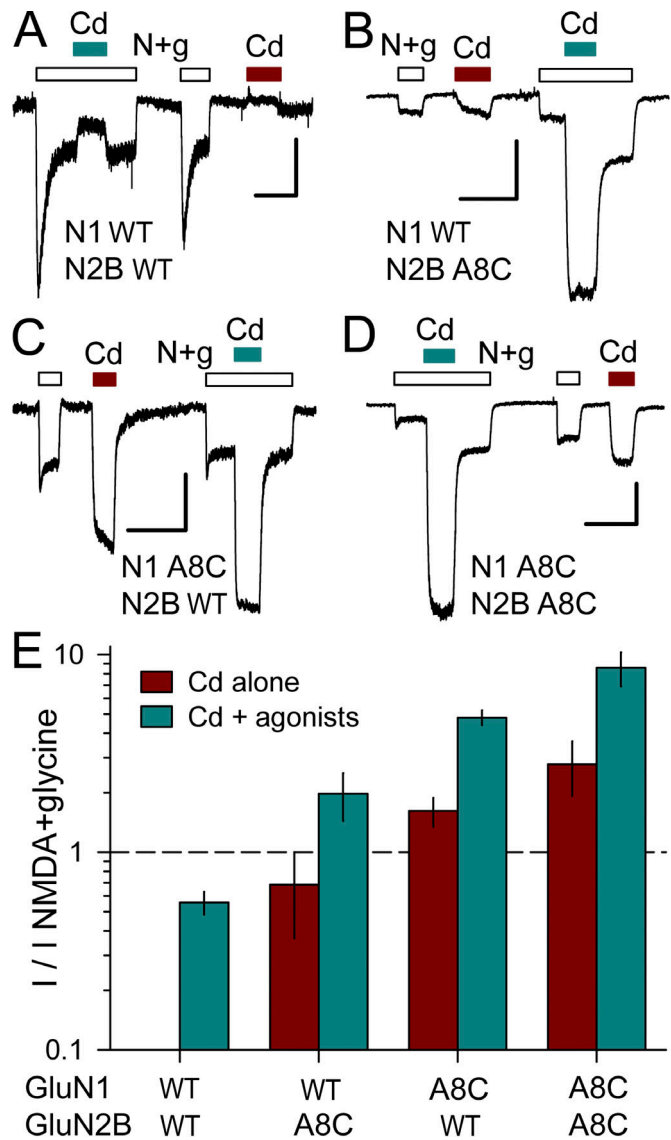
Figure 8. **Cd activation of A8C substituted NMDA receptors. (A–D)** Whole-cell currents evoked by 10 µM NMDA + 10 µM glycine (open bars), 50 µM Cd alone (red bars), or Cd together with agonists (cyan bars) in HEK293 cells cotransfected with WT GluN1 and GluN2B (A), GluN1 WT and GluN2B A8C (B), GluN1 A8C and GluN2B WT (C), or GluN1 A8C and GluN2B A8C (D). Holding potential is −80 mV. Scale bars represent 300 pA and 30 ms. **(E)** Current evoked by 50 µM Cd alone (red bars) or together with 10 µM NMDA plus 10 µM glycine (cyan bars) as a fraction of the current evoked by agonist alone (mean ± SEM, 10–48 cells per construct). Note the log scale. All of the mutant combinations were significantly different from WT but were not significantly different from each other (ANOVA on ranks with post hoc Dunn's test).

or by Cd together with the agonists also were strongly blocked by Mg at negative potentials in cells expressing receptors with A8C substitution in the N1 subunit, the N2B subunit or both N1 and N2B (Fig. 11 E). Thus, replacement of A8 with Cys and interaction with Cd do not prevent the movement of Mg ions past the bundle crossing and into the central cavity at negative potentials (see Kashiwagi et al., 2002; Yuan et al., 2005). Slight potentiation by Mg at positive potentials (Paoletti et al., 1995) was also observed for receptors that included the N2B A8C
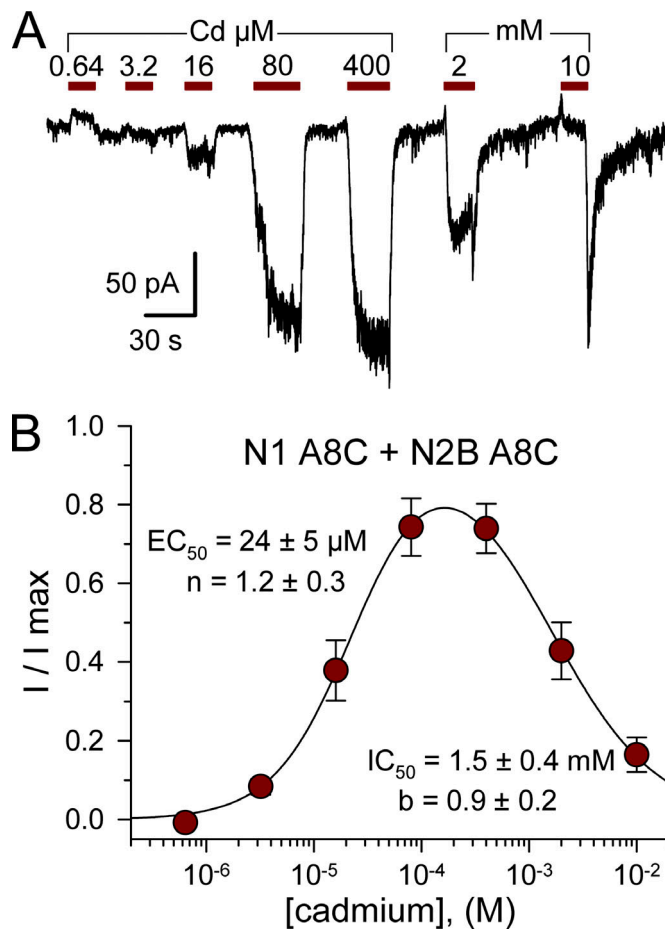
Figure 9. **Concentration dependence of N1 A8C + N2B A8C activation.** **(A)** Whole-cell currents evoked by increasing concentrations of Cd from 640 nM to 10 mM in an HEK293 cell cotransfected with GluN1 A8C and GluN2B A8C. **(B)** Steady-state current recoded during exposure to each Cd concentration as a fraction of the maximal Cd-evoked response (mean ± SEM; 18 cells). Smooth curve is the best fit of $I/I\ max = \{1 / [1 + (EC_{50} / [Cd])^n]\} / [1+([Cd]/IC_{50})^b]$, where EC_{50} and IC_{50} are the Cd concentrations producing half-maximal activation and inhibition, respectively; n and b are the slope factors for activation and inhibition.

mutant subunit together with either WT GluN1 or GluN1 A8C (Fig. 11 E). Interestingly, we observed significantly greater potentiation by 1 mM Mg for the combination of GluN1 A8C coexpressed with WT GluN2B (Fig. 11, B and E), suggesting a specific linkage between GluN1 residues at the bundle crossing and the positive allosteric modulation site within the N1/N2B ATD dimer interface where Mg and polyamines bind (Mony et al., 2011). As shown in Fig. 11, D and E, exposure to 1 mM Mg yielded no potentiation of agonist evoked currents at positive potentials in cells cotransfected with GluN1 A8C and WT GluN2A, which confirms that the strong Mg potentiation observed for the N1 A8C + N2B WT combination involves a similar mechanism to that previously reported for WT N1 + N2B receptors (Paoletti et al., 1995; Mony et al., 2011). Additional experiments demonstrated intact voltage-dependent Mg block in cells expressing receptors that included the N1L10C or N2BM10C subunits (Fig. S5).

Acidic pH reduces Cd activation

Potentiation of N1/N2B NMDA receptors by Mg or polyamines involves relief of tonic inhibition by protons (Traynelis et al., 1995; Paoletti et al., 1995; Mony et al., 2011). Recent structural analysis (Jalali-Yazdi et al., 2018; Regan et al., 2018; Zhang et al., 2018) confirms earlier evidence (Gielen et al., 2009; Yuan et al., 2009) that conformational changes in the ATD and LBD underlie proton inhibition. In addition, however, mutations in the SY-TANLAAF motif of both N1 and N2 subunits also can alter the potency of proton inhibition (Low et al., 2003), highlighting the mechanistic link between agonist binding and the bundle-crossing gate (Ladislav et al., 2018; Wilding and Huettner, 2019). To test whether protons influence the action of Cd on A8C or L10C mutant receptors we recorded currents during exposure to NMDA and glycine alone or together with Cd at pH 6.6 and 8.0 in cells cotransfected with N1 A8C or N1 L10C with WT N2A or N2B. As shown in Fig. 12, agonist-evoked currents displayed robust enhancement by Cd at pH 8.0 but no significant potentiation by Cd coapplication at pH 6.6. Thus, Cd does not act by overcoming proton inhibition but instead exhibits inhibition by protons as is observed for channel activation by agonist (Traynelis et al., 1995).

Lowering the pH might reduce Cd activation by protonation of the same sites that underlie inhibition of agonist-gated currents in WT receptors (Traynelis et al., 2010) or might reflect a reduction in Cd coordination via direct protonation of the substituted Cys side chains (Grimsley at al., 2009). To test whether pH dependence of Cd activation was restricted to NMDA receptors, we evaluated Cys-substituted AMPA and kainate receptors at pH 6.6, where WT receptors exhibit modest proton inhibition of agonist-gated currents (Ihle and Patneau, 2000; Lei et al., 2001; Mott et al., 2003). Whole-cell currents evoked by 100 µM kainate in cells expressing A8C or L10C mutant AMPA or kainate receptors were smaller at pH 6.6 than at pH 7.4. Moreover, currents evoked by Cd in the A8C mutants or by kainate plus Cd in the L10C mutants were also significantly reduced at pH 6.6 (Fig. S6), both in absolute terms as well as relative to agonist-evoked current. Together, these results demonstrate substantial proton inhibition of Cd-evoked currents in all three iGluR subtypes with A8C or L10C mutations.

Discussion

NMDA receptors exhibit physiological and pharmacological properties distinct from AMPA and kainate receptors, which are often grouped together as non-NMDA receptors owing to their functional similarities and higher level of sequence identity (Traynelis et al., 2010). All three iGluRs share a common modular organization and basic gating mechanism whereby agonist binding changes the LBD conformation, exerting tension on short linker segments that deform the M3 helix bundle crossing and open a passage for ions and water into the pore (Twomey and Sobolevsky, 2018). Early work revealed that side chains in the conserved M3 SYTANLAAF sequence contribute to the bundle crossing occlusion zone of all iGluRs (Zuo et al., 1997; Kohda et al., 2000; Taverna et al., 2000; Wollmuth et al., 2000); however, additional studies delineated motifs and specific
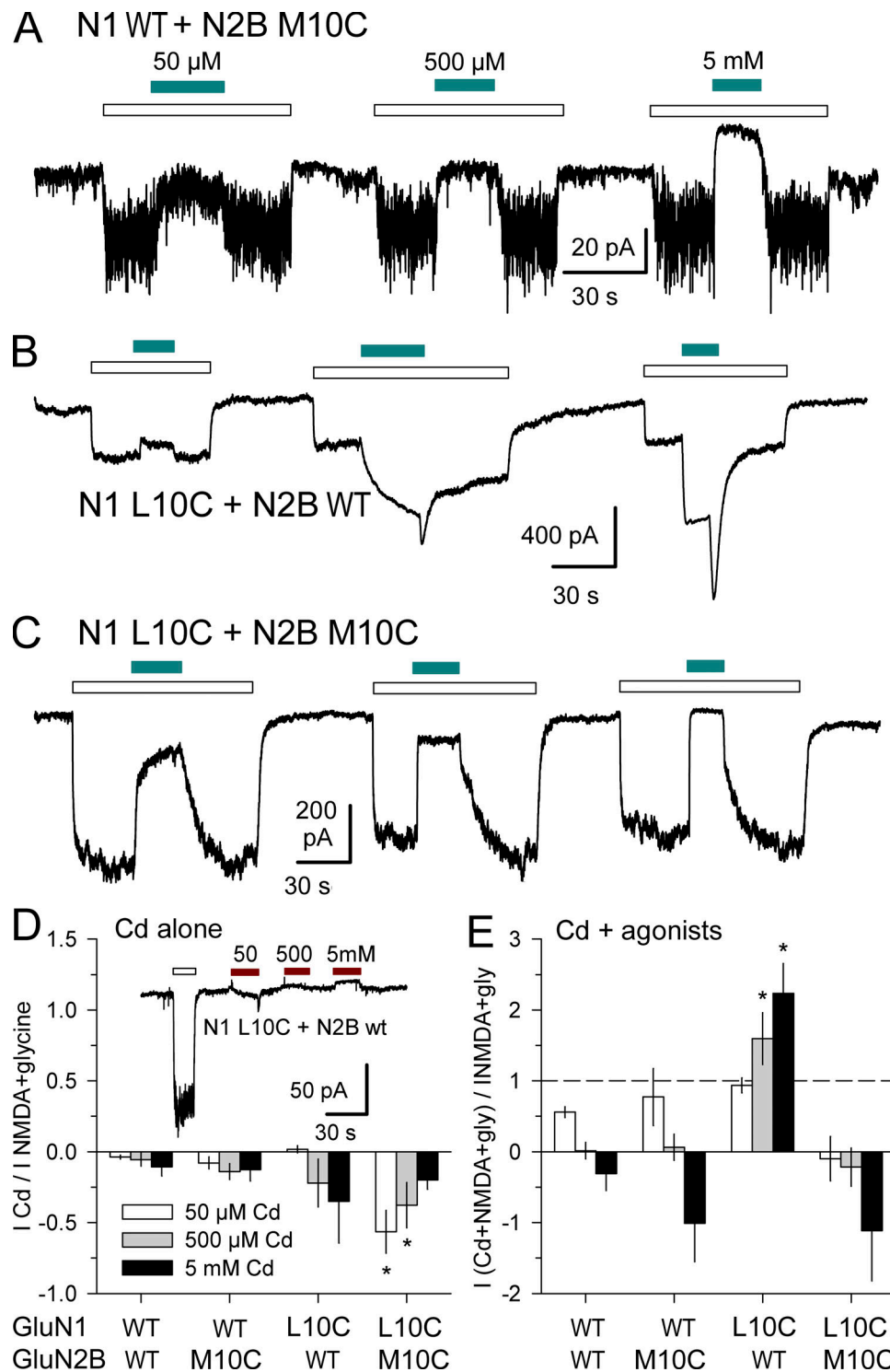
Figure 10. **Subunit-dependent potentiation for Cys substitution at the +10 position. (A–C)** Whole-cell currents evoked by 10 µM NMDA + 10 µM glycine (open bars) alone or together with coapplication of 50 µM, 500 µM, or 5 mM Cd (cyan bars, left to right) in HEK293 cells transfected with GluN1 WT + GluN2B M10C (A), N1 L10C + N2B WT (B), or N1 L10C + N2B M10C (C). Holding potential is −80 mV. **(D and E)** Current recorded during exposure to Cd alone (D) or Cd together with agonists (E) plotted as a fraction of current evoked by agonist alone (mean ± SEM, 4–21 cells per condition). Asterisks denote significant difference from WT (one-way ANOVA with post hoc Dunn's test). **(D)** Inset shows Application of 50 µM, 500 µM, and 5 mM Cd alone (red bars) caused little change in holding current in a cell transfected with N1L10C + N2B WT.
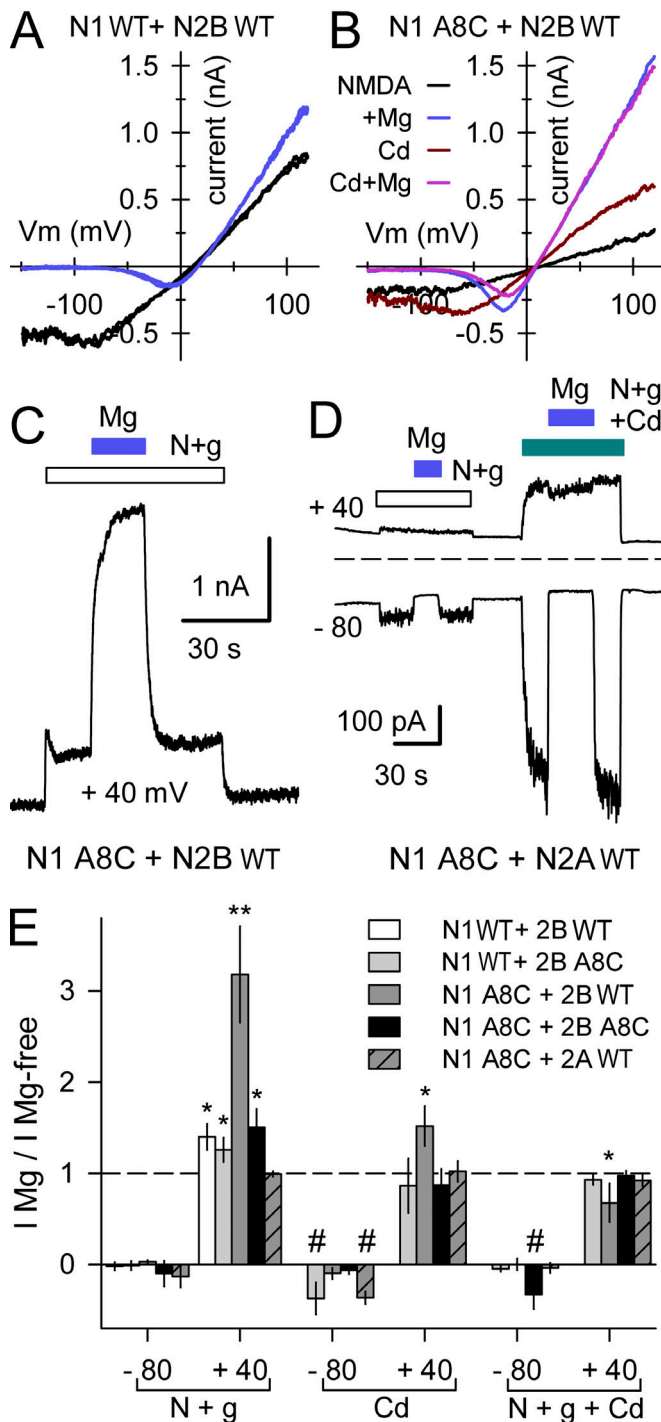
Figure 11. **Mg block and potentiation. (A and B)** Current–voltage relations recorded during voltage ramps from −150 to +120 mV in cells transfected with N2B WT and either N1 WT (A) or N1 A8C (B). **(C)** Outward current evoked by NMDA + glycine (open bar) and with 1 mM Mg (blue bar) while holding steady at +40 mV in an HEK293 cell transfected with N1 A8C + N2B WT. **(D)** Current evoked by NMDA + glycine alone (open bar) or with 50 µM Cd (cyan bar) in a cell expressing N1 A8C and N2A WT. Traces depict currents averaged over 2.5-ms intervals while holding at −80 mV and during 50-ms steps to +40 mV delivered at 5 Hz. Blue bars indicate coapplication of 1 mM Mg. **(E)** Summary plot of currents (mean ± SEM, 5–16 cells per construct) evoked at −80 and +40 mV in the presence of 1 mM Mg as a fraction of current in Mg-free solution for NMDA + glycine and for Cd alone or together with agonist. * denotes significant difference from $I_{Mg}/I_{Mg-free}$ = 1 (*t* test).

residues within the LBD-TMD linkers and in the extracellular portions of M1, M3, and M4 that underlie many of the important functional and pharmacological differences between NMDA and non-NMDA receptors (Watanabe et al., 2002; Low et al., 2003; Chang and Kuo, 2008; Alsaloum et al., 2016; Ladislav et al., 2018; Perszyk et al., 2018).

Our results with Cys substituted AMPA and NMDA receptors in the present study, together with our earlier work on GluK2 kainate receptor A8C and L10C mutations (Wilding and Huettner, 2019), identify a shared mechanism for prying open iGluR bundle crossing gates independent of agonist binding to the LBDs (Wollmuth, 2019). For all three iGluR subtypes, exposure to Cd produced rapid and reversible activation of receptors that included subunits with the A8C substitution. The potency of activation for A8C mutant receptors, with half-maximal Cd concentrations in the range of 5–25 µM, is consistent with Cd coordination by at least two side chains (Puljung and Zagotta, 2011). In contrast, the higher Cd concentrations required for activation of receptors with L10C substitutions indicate a lower affinity interaction that may not require multiple coordinating residues (Wilding and Huettner, 2019). Our results also show that activation by Cd does not require Cys substitution on all four of the subunits within a tetrameric iGluR. Potency for activation by Cd was lower for receptors with fewer than four mutant subunits, as predicted by simple kinetic models with different numbers of binding sites (Wilding and Huettner, 2019). Importantly, Cd consistently activated A8C or L10C substituted heteromeric receptors that likely contain two mutant subunits alternating with two WT subunits resulting in Cys substitutions arranged diagonally across the pore axis (Greger and Mayer 2019).

For the A8C mutation, we do not know if a single Cd coordinates with both substituted Cys residues, but such an arrangement would place the coordinated Cd directly along the pore axis (Wollmuth 2019) and would likely restrict the M3 helices from splaying apart (Wilding and Huettner, 2019). Instead, each substituted Cys may coordinate Cd with other native residues nearby (Zhou et al., 2015; Tu et al., 2016). Our experiments with A8C-substituted NMDA receptors demonstrate that Mg coapplication produces voltage-dependent block of agonist evoked currents (Nowak et al., 1984; Mayer et al., 1984) as well as current elicited by Cd alone or Cd together with agonist, suggesting that Cd coordination does not hinder passage of Mg into the central cavity. This result is consistent with previous work (Yuan et al., 2005; Chang and Kuo, 2008) showing persistence of voltage-dependent Mg block for NMDA receptors with bundle-crossing Cys substitutions after treatment with MTSEA, a sulfhydryl-reactive agent that modifies free Cys residues to yield a positively charged side chain approximately the size of lysine (Akabas, 2015). Thus, addition of positive charge at the bundle crossing does not preclude the passage of cations, including larger polyvalent cations such as Mg.

** denotes significant difference from N1 WT + N2B WT (one-way ANOVA with post hoc Dunn's test). # indicates significant difference from $I_{Mg}/I_{Mg-free}$ = 0 (*t* test).
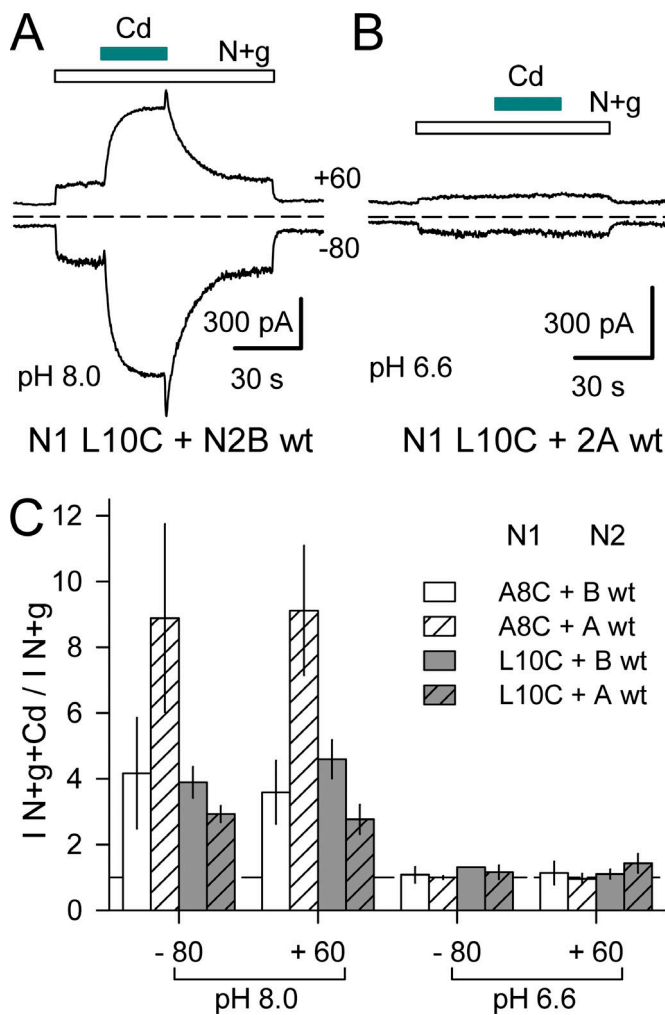
Figure 12. **Protons inhibit Cd potentiation of NMDA receptors with M3 helix Cys substitutions. (A and B)** Whole-cell currents evoked at pH 8.0 (A) or pH 6.6 (B) by 10 µM NMDA and glycine (open bars) alone or together with 400 µM Cd (cyan bars) in HEK293 cells cotransfected with N1 L10C and either N2B WT (A) or N2A WT (B). **(C)** Summary plot of currents (mean ± SEM, four to seven cells per construct) evoked at −80 and +60 mV by NMDA + glycine + Cd as a fraction of NMDA + glycine alone, at pH 8.0 or pH 6.6. The difference between pH 8.0 and pH 6.6 was significant for each construct combination (paired t test). In addition, at pH 8.0, the (I_{N+g+Cd} / I_{N+g}) ratio was significantly larger for N1A8C coexpressed with N2A WT than with N2B WT (t test).

Initial evidence that the residue at position 8 is important for iGluR gating came from study of Lurcher mutant mice, which have a missense mutation that introduces an A8T substitution in the orphan delta-2 iGluR subunit (Zuo et al., 1997). Cells expressing this mutant subunit exhibit constitutive channel activity (Kohda et al., 2000; Wollmuth et al., 2000; Schwarz et al., 2001). Homologous A8T substitution in AMPA and kainate receptor subunits reduces desensitization, slows deactivation, increases affinity for agonists, and promotes variable levels of constitutive channel opening (Kohda et al., 2000; Taverna et al., 2000; Klein and Howe, 2004). For NMDA receptors, A8T substitution in either GluN1 or GluN2 reduces receptor inhibition by protons (Low et al., 2003), but A8 replacement in GluN2 has negligible effect on receptor activation, desensitization, or

deactivation, and A8 substitution in GluN1 causes only modest changes in these parameters (Kohda et al., 2000; Hu and Zheng, 2005; Murthy et al., 2012) compared with much larger effects produced by GluN1 or GluN2 substitutions at the adjacent A7 position (Jones et al., 2002; Yuan et al., 2005; Blanke and VanDongen, 2008; Murthy et al., 2012; Tu and Kuo, 2015) or other nearby residues (Chang and Kuo, 2008; Ladislav et al., 2018).

Our results demonstrate Cd activation for NMDA receptors with A8C substitution to both the N1 and N2 subunit or to either subunit alone, but we also identified two unique features for receptors that included WT GluN2 coexpressed with A8C or L10C substitutions only on the N1 subunit. First, Cd enhanced agonist-evoked current in cells coexpressing N1 L10C together with WT N2B or N2A but inhibited currents in cells that received N2B M10C together with either N1 L10C or N1 WT. Second, exposure to Mg produced significantly greater potentiation in cells cotransfected with N1A8C and N2B WT, whereas coexpression of N2B A8C with either N1 A8C or N1 WT exhibited the same potentiation as receptors in which both N1 and N2B subunits were WT (Paoletti et al., 1995). It is notable that in both cases where Cys-substituted N1 subunits yield a novel phenotype when coexpressed with WT N2B, the corresponding Cys-substituted N2B phenotype dominates when coexpressed with either WT or mutant N1. These differences likely reflect the asymmetric conformations of N1 and N2 subunits within the heterotetramer (Karakas and Furukawa, 2014; Lee et al., 2014). GluN1 subunits adopt the A/C conformation (Sobolevsky et al., 2009) with linkers from M3 extending up toward the LBD, whereas GluN2 subunits are in the B/D conformation, with their M3 linkers oriented almost perpendicular to the pore axis. Increasing evidence suggests that subunits in the B/D conformation play the major role in control of gating (Murthy et al., 2012; Kazi et al., 2014; Tu and Kuo, 2015) consistent with the greater deformation observed for B/D subunit M3 helices when iGluRs open (Chen et al., 2017; Twomey et al., 2017). Importantly, receptors formed by cotransfection N1A8C with N2A WT were activated by Cd but displayed no potentiation by Mg as previously shown for N1 WT/N2A WT receptors (Paoletti et al., 1995). This result demonstrates that receptor activation or potentiation by Cd is distinct from potentiation by Mg because N1 A8C/N2A WT receptors respond to Cd but lack potentiation by Mg. In addition, our results suggest that greater Mg potentiation observed for N1 A8C/N2B WT likely involves an enhancement of the same N2B-specific relief from proton inhibition that underlies Mg potentiation of WT N1/N2B diheteromers (Mony et al., 2011). Our results also show that in contrast to Mg, the activation of Cys-substituted iGluRs by Cd is strongly inhibited by protons, with Cd having minimal effect on A8C or L10C mutant AMPA, kainate, or NMDA receptors at pH 6.6.

Numerous previous studies have delineated the changes induced by γ-2 TARP coexpression on AMPA receptor agonist-evoked currents, including increases in agonist potency and partial agonist efficacy (Jackson and Nicoll, 2011; Greger et al., 2017). Our results reveal substantial effects of γ-2 TARP on Cd activation of M3 mutant homomeric and heteromeric AMPA receptors. TARP coexpression reduced allosteric potentiation of

agonist-gated currents by Cd for GluA1 A8C or L10C and protected receptors with the A8C mutation from modification by MTSEA. In contrast, for receptors with the L10C mutation, treatment with MTSEA produced a larger decline in activation by agonist and/or Cd in cells cotransfected with γ-2 TARP than in cells expressing GluA1 L10C alone. In addition, TARP coexpression increased the apparent affinity for Cd activation of GluA1 L10C and promoted inhibition by higher doses of Cd compared with receptors expressed without γ-2 TARP.

Conclusions

Our results demonstrate that AMPA, NMDA, and kainate receptor channels with specific M3 Cys substitutions can be pried open by exposure to cadmium independent of agonist occupancy. Cd activates channels with A8C substitution to subunits in either the A/C or B/D conformation, despite asymmetry in the heteromeric NMDA receptor TMD (Sobolevsky et al., 2007; Karakas and Furukawa, 2014; Lee et al., 2014) and marked asymmetry in the arrangement of distal M3 residues in the open-state structure of homomeric AMPA receptors (Chen et al., 2017; Twomey et al., 2017). For NMDA receptors, but not AMPA or kainate receptors, we observe asymmetric effects of Cd on subunits with Cys substitution at the +10 position. Consistent with previous work (Murthy et al., 2012; Kazi et al., 2014; Tu and Kuo, 2015), the GluN2 subunit was dominant over GluN1. Surprisingly, however, GluN2 dominance was most striking in cases where novel phenotypes produced by GluN1 L10C were suppressed by coexpression of GluN2B M10C. Further work on these and other (Hu et al., 2016) mutations near the bundle crossing may aid in the design of therapeutic agents by revealing structural rearrangements that underlie novel channel open conformations.

Acknowledgments

References

Akabas, M.H. 2015. Cysteine Modification: Probing Channel Structure, Function and Conformational Change. *Adv. Exp. Med. Biol.* 869:25–54. https://doi.org/10.1007/978-1-4939-2845-3_3

Alsaloum, M., R. Kazi, Q. Gan, J. Amin, and L.P. Wollmuth. 2016. A Molecular Determinant of Subtype-Specific Desensitization in Ionotropic Glutamate Receptors. *J. Neurosci.* 36:2617–2622. https://doi.org/10.1523/JNEUROSCI.2667-15.2016

Bano, D., and M. Ankarcrona. 2018. Beyond the critical point: An overview of excitotoxicity, calcium overload and the downstream consequences. *Neurosci. Lett.* 663:79–85. https://doi.org/10.1016/j.neulet.2017.08.048

Blanke, M.L., and A.M. VanDongen. 2008. The NR1 M3 domain mediates allosteric coupling in the N-methyl-D-aspartate receptor. *Mol. Pharmacol.* 74:454–465. https://doi.org/10.1124/mol.107.044115

Boulter, J., M. Hollmann, A. O'Shea-Greenfield, M. Hartley, E. Deneris, C. Maron, and S. Heinemann. 1990. Molecular cloning and functional expression of glutamate receptor subunit genes. *Science.* 249:1033–1037. https://doi.org/10.1126/science.2168579

Chang, H.R., and C.C. Kuo. 2008. The activation gate and gating mechanism of the NMDA receptor. *J. Neurosci.* 28:1546–1556. https://doi.org/10.1523/JNEUROSCI.3485-07.2008

Chen, S., Y. Zhao, Y. Wang, M. Shekhar, E. Tajkhorshid, and E. Gouaux. 2017. Activation and Desensitization Mechanism of AMPA Receptor-TARP Complex by Cryo-EM. *Cell.* 170:1234–1246.e14. https://doi.org/10.1016/j.cell.2017.07.045

Fernández-Marmiesse, A., H. Kusumoto, S. Rekarte, I. Roca, J. Zhang, S.J. Myers, S.F. Traynelis, M.L. Couce, L. Gutierrez-Solana, and H. Yuan. 2018. A novel missense mutation in GRIN2A causes a nonepileptic neurodevelopmental disorder. *Mov. Disord.* 33:992–999. https://doi.org/10.1002/mds.27315

Fisher, J.L., and D.D. Mott. 2011. Distinct functional roles of subunits within the heteromeric kainate receptor. *J. Neurosci.* 31:17113–17122. https://doi.org/10.1523/JNEUROSCI.3685-11.2011

Fry, A.E., K.A. Fawcett, N. Zelnik, H. Yuan, B.A.N. Thompson, L. Shemer-Meiri, T.D. Cushion, H. Mugalaasi, D. Sims, N. Stoodley, et al. 2018. De novo mutations in GRIN1 cause extensive bilateral polymicrogyria. *Brain.* 141:698–712. https://doi.org/10.1093/brain/awx358

Gielen, M., B. Siegler Retchless, L. Mony, J.W. Johnson, and P. Paoletti. 2009. Mechanism of differential control of NMDA receptor activity by NR2 subunits. *Nature.* 459:703–707. https://doi.org/10.1038/nature07993

Gleichman, A.J., L.A. Spruce, J. Dalmau, S.H. Seeholzer, and D.R. Lynch. 2012. Anti-NMDA receptor encephalitis antibody binding is dependent on amino acid identity of a small region within the GluN1 amino terminal domain. *J. Neurosci.* 32:11082–11094. https://doi.org/10.1523/JNEUROSCI.0064-12.2012

Greger, I.H., and M.L. Mayer. 2019. Structural biology of glutamate receptor ion channels: towards an understanding of mechanism. *Curr. Opin. Struct. Biol.* 57:185–195. https://doi.org/10.1016/j.sbi.2019.05.004

Greger, I.H., J.F. Watson, and S.G. Cull-Candy. 2017. Structural and Functional Architecture of AMPA-Type Glutamate Receptors and Their Auxiliary Proteins. *Neuron.* 94:713–730. https://doi.org/10.1016/j.neuron.2017.04.009

Grimsley, G.R., J.M. Scholtz, and C.N. Pace. 2009. A summary of the measured pK values of the ionizable groups in folded proteins. *Protein Sci.* 18:247–251.

Guzmán, Y.F., K. Ramsey, J.R. Stolz, D.W. Craig, M.J. Huentelman, V. Narayanan, and G.T. Swanson. 2017. A gain-of-function mutation in the GRIK2 gene causes neurodevelopmental deficits. *Neurol. Genet.* 3:e129. https://doi.org/10.1212/NXG.0000000000000129

Hansen, K.B., K.K. Ogden, H. Yuan, and S.F. Traynelis. 2014. Distinct functional and pharmacological properties of Triheteromeric GluN1/GluN2A/GluN2B NMDA receptors. *Neuron.* 81:1084–1096. https://doi.org/10.1016/j.neuron.2014.01.035

Hollmann, M., J. Boulter, C. Maron, L. Beasley, J. Sullivan, G. Pecht, and S. Heinemann. 1993. Zinc potentiates agonist-induced currents at certain splice variants of the NMDA receptor. *Neuron.* 10:943–954. https://doi.org/10.1016/0896-6273(93)90209-A

Hu, B., and F. Zheng. 2005. Differential effects on current kinetics by point mutations in the lurcher motif of NR1/NR2A receptors. *J. Pharmacol. Exp. Ther.* 312:899–904. https://doi.org/10.1124/jpet.104.077388

Hu, C., W. Chen, S.J. Myers, H. Yuan, and S.F. Traynelis. 2016. Human GRIN2B variants in neurodevelopmental disorders. *J. Pharmacol. Sci.* 132:115–121. https://doi.org/10.1016/j.jphs.2016.10.002

Huettner, J.E. 2015. Glutamate receptor pores. *J. Physiol.* 593:49–59. https://doi.org/10.1113/jphysiol.2014.272724

Ihle, E.C., and D.K. Patneau. 2000. Modulation of alpha-amino-3-hydroxy-5-methyl-4-isoxazolepropionic acid receptor desensitization by extracellular protons. *Mol. Pharmacol.* 58:1204–1212. https://doi.org/10.1124/mol.58.6.1204

Jackson, A.C., and R.A. Nicoll. 2011. The expanding social network of ionotropic glutamate receptors: TARPs and other transmembrane auxiliary subunits. *Neuron.* 70:178–199. https://doi.org/10.1016/j.neuron.2011.04.007

Jalali-Yazdi, F., S. Chowdhury, C. Yoshioka, and E. Gouaux. 2018. Mechanisms for Zinc and Proton Inhibition of the GluN1/GluN2A NMDA Receptor. *Cell.* 175:1520–1532.e15. https://doi.org/10.1016/j.cell.2018.10.043

Johnson, J.W., and P. Ascher. 1987. Glycine potentiates the NMDA response in cultured mouse brain neurons. *Nature.* 325:529–531. https://doi.org/10.1038/325529a0

Jones, K.S., H.M. VanDongen, and A.M. VanDongen. 2002. The NMDA receptor M3 segment is a conserved transduction element coupling ligand binding to channel opening. *J. Neurosci.* 22:2044–2053. https://doi.org/10.1523/JNEUROSCI.22-06-02044.2002

Karakas, E., and H. Furukawa. 2014. Crystal structure of a heterotetrameric NMDA receptor ion channel. *Science.* 344:992–997. https://doi.org/10.1126/science.1251915

Kashiwagi, K., T. Masuko, C.D. Nguyen, T. Kuno, I. Tanaka, K. Igarashi, and K. Williams. 2002. Channel blockers acting at N-methyl-D-aspartate receptors: differential effects of mutations in the vestibule and ion channel pore. *Mol. Pharmacol.* 61:533–545. https://doi.org/10.1124/mol.61.3.533

Kazi, R., J. Dai, C. Sweeney, H.X. Zhou, and L.P. Wollmuth. 2014. Mechanical coupling maintains the fidelity of NMDA receptor-mediated currents. *Nat. Neurosci.* 17:914–922. https://doi.org/10.1038/nn.3724

Kleckner, N.W., and R. Dingledine. 1988. Requirement for glycine in activation of NMDA-receptors expressed in Xenopus oocytes. *Science.* 241:835–837. https://doi.org/10.1126/science.2841759

Klein, R.M., and J.R. Howe. 2004. Effects of the lurcher mutation on GluR1 desensitization and activation kinetics. *J. Neurosci.* 24:4941–4951. https://doi.org/10.1523/JNEUROSCI.0660-04.2004

Kohda, K., Y. Wang, and M. Yuzaki. 2000. Mutation of a glutamate receptor motif reveals its role in gating and delta2 receptor channel properties. *Nat. Neurosci.* 3:315–322. https://doi.org/10.1038/73877

Kuner, T., P.H. Seeburg, and H.R. Guy. 2003. A common architecture for K+ channels and ionotropic glutamate receptors? *Trends Neurosci.* 26:27–32. https://doi.org/10.1016/S0166-2236(02)00010-3

Ladislav, M., J. Cerny, J. Krusek, M. Horak, A. Balik, and L. Vyklicky. 2018. The LILI Motif of M3-S2 Linkers Is a Component of the NMDA Receptor Channel Gate. *Front. Mol. Neurosci.* 11:113. https://doi.org/10.3389/fnmol.2018.00113

Lee, C.H., W. Lü, J.C. Michel, A. Goehring, J. Du, X. Song, and E. Gouaux. 2014. NMDA receptor structures reveal subunit arrangement and pore architecture. *Nature.* 511:191–197. https://doi.org/10.1038/nature13548

Lei, S., B.A. Orser, G.R. Thatcher, J.N. Reynolds, and J.F. MacDonald. 2001. Positive allosteric modulators of AMPA receptors reduce proton-induced receptor desensitization in rat hippocampal neurons. *J. Neurophysiol.* 85:2030–2038. https://doi.org/10.1152/jn.2001.85.5.2030

Li, D., H. Yuan, X.R. Ortiz-Gonzalez, E.D. Marsh, L. Tian, E.M. McCormick, G.J. Kosobucki, W. Chen, A.J. Schulien, R. Chiavacci, et al. 2016. GRIN2D Recurrent De Novo Dominant Mutation Causes a Severe Epileptic Encephalopathy Treatable with NMDA Receptor Channel Blockers. *Am. J. Hum. Genet.* 99:802–816. https://doi.org/10.1016/j.ajhg.2016.07.013

Lopez, M.N., T.J. Wilding, and J.E. Huettner. 2013. Q/R site interactions with the M3 helix in GluK2 kainate receptor channels revealed by thermodynamic mutant cycles. *J. Gen. Physiol.* 142:225–239. https://doi.org/10.1085/jgp.201311000

Low, C.M., P. Lyuboslavsky, A. French, P. Le, K. Wyatte, W.H. Thiel, E.M. Marchan, K. Igarashi, K. Kashiwagi, K. Gernert, et al. 2003. Molecular determinants of proton-sensitive N-methyl-D-aspartate receptor gating. *Mol. Pharmacol.* 63:1212–1222. https://doi.org/10.1124/mol.63.6.1212

Mayer, M.L., G.L. Westbrook, and P.B. Guthrie. 1984. Voltage-dependent block by Mg2+ of NMDA responses in spinal cord neurones. *Nature.* 309:261–263. https://doi.org/10.1038/309261a0

Mayer, M.L., L. Vyklicky Jr., and G.L. Westbrook. 1989. Modulation of excitatory amino acid receptors by group IIB metal cations in cultured mouse hippocampal neurones. *J. Physiol.* 415:329–350. https://doi.org/10.1113/jphysiol.1989.sp017724

Mony, L., S. Zhu, S. Carvalho, and P. Paoletti. 2011. Molecular basis of positive allosteric modulation of GluN2B NMDA receptors by polyamines. *EMBO J.* 30:3134–3146. https://doi.org/10.1038/emboj.2011.203

Mott, D.D., M.S. Washburn, S. Zhang, and R.J. Dingledine. 2003. Subunit-dependent modulation of kainate receptors by extracellular protons and polyamines. *J. Neurosci.* 23:1179–1188. https://doi.org/10.1523/JNEUROSCI.23-04-01179.2003

Murthy, S.E., T. Shogan, J.C. Page, E.M. Kasperek, and G.K. Popescu. 2012. Probing the activation sequence of NMDA receptors with lurcher mutations. *J. Gen. Physiol.* 140:267–277. https://doi.org/10.1085/jgp.201210786

Nowak, L., P. Bregestovski, P. Ascher, A. Herbet, and A. Prochiantz. 1984. Magnesium gates glutamate-activated channels in mouse central neurones. *Nature.* 307:462–465. https://doi.org/10.1038/307462a0

Paoletti, P., J. Neyton, and P. Ascher. 1995. Glycine-independent and subunit-specific potentiation of NMDA responses by extracellular Mg2+. *Neuron.* 15:1109–1120. https://doi.org/10.1016/0896-6273(95)90099-3

Pérez-Otaño, I., R.S. Larsen, and J.F. Wesseling. 2016. Emerging roles of GluN3-containing NMDA receptors in the CNS. *Nat. Rev. Neurosci.* 17:623–635. https://doi.org/10.1038/nrn.2016.92

Perszyk, R., B.M. Katzman, H. Kusumoto, S.A. Kell, M.P. Epplin, Y.A. Tahirovic, R.L. Moore, D. Menaldino, P. Burger, D.C. Liotta, and S.F. Traynelis. 2018. An NMDAR positive and negative allosteric modulator series share a binding site and are interconverted by methyl groups. *eLife.* 7:e34711. https://doi.org/10.7554/eLife.34711

Puljung, M.C., and W.N. Zagotta. 2011. Labeling of specific cysteines in proteins using reversible metal protection. *Biophys. J.* 100:2513–2521. https://doi.org/10.1016/j.bpj.2011.03.063

Regan, M.C., T. Grant, M.J. McDaniel, E. Karakas, J. Zhang, S.F. Traynelis, N. Grigorieff, and H. Furukawa. 2018. Structural Mechanism of Functional Modulation by Gene Splicing in NMDA Receptors. *Neuron.* 98:521–529.e3. https://doi.org/10.1016/j.neuron.2018.03.034

Rosenmund, C., Y. Stern-Bach, and C.F. Stevens. 1998. The tetrameric structure of a glutamate receptor channel. *Science.* 280:1596–1599. https://doi.org/10.1126/science.280.5369.1596

Salussolia, C.L., Q. Gan, R. Kazi, P. Singh, J. Allopenna, H. Furukawa, and L.P. Wollmuth. 2013. A eukaryotic specific transmembrane segment is required for tetramerization in AMPA receptors. *J. Neurosci.* 33:9840–9845. https://doi.org/10.1523/JNEUROSCI.2626-12.2013

Schwarz, M.K., V. Pawlak, P. Osten, V. Mack, P.H. Seeburg, and G. Köhr. 2001. Dominance of the lurcher mutation in heteromeric kainate and AMPA receptor channels. *Eur. J. Neurosci.* 14:861–868. https://doi.org/10.1046/j.0953-816x.2001.01705.x

Smith, T.C., and J.R. Howe. 2000. Concentration-dependent substate behavior of native AMPA receptors. *Nat. Neurosci.* 3:992–997. https://doi.org/10.1038/79931

Sobolevsky, A.I., M.V. Yelshansky, and L.P. Wollmuth. 2003. Different gating mechanisms in glutamate receptor and K+ channels. *J. Neurosci.* 23:7559–7568. https://doi.org/10.1523/JNEUROSCI.23-20-07559.2003

Sobolevsky, A.I., M.V. Yelshansky, and L.P. Wollmuth. 2004. The outer pore of the glutamate receptor channel has 2-fold rotational symmetry. *Neuron.* 41:367–378. https://doi.org/10.1016/S0896-6273(04)00008-X

Sobolevsky, A.I., M.L. Prodromou, M.V. Yelshansky, and L.P. Wollmuth. 2007. Subunit-specific contribution of pore-forming domains to NMDA receptor channel structure and gating. *J. Gen. Physiol.* 129:509–525. https://doi.org/10.1085/jgp.200609718

Sobolevsky, A.I., M.P. Rosconi, and E. Gouaux. 2009. X-ray structure, symmetry and mechanism of an AMPA-subtype glutamate receptor. *Nature.* 462:745–756. https://doi.org/10.1038/nature08624

Swanson, G.T., T. Green, R. Sakai, A. Contractor, W. Che, H. Kamiya, and S.F. Heinemann. 2002. Differential activation of individual subunits in heteromeric kainate receptors. *Neuron.* 34:589–598. https://doi.org/10.1016/S0896-6273(02)00676-1

Swartz, K.J., W.J. Koroshetz, A.H. Rees, and J.E. Huettner. 1992. Competitive antagonism of glutamate receptor channels by substituted benzazepines in cultured cortical neurons. *Mol. Pharmacol.* 41:1130–1141.

Taverna, F., Z.G. Xiong, L. Brandes, J.C. Roder, M.W. Salter, and J.F. MacDonald. 2000. The Lurcher mutation of an alpha-amino-3-hydroxy-5-methyl- 4-isoxazolepropionic acid receptor subunit enhances potency of glutamate and converts an antagonist to an agonist. *J. Biol. Chem.* 275:8475–8479. https://doi.org/10.1074/jbc.275.12.8475

Terhag, J., K. Gottschling, and M. Hollmann. 2010. The Transmembrane Domain C of AMPA Receptors is Critically Involved in Receptor Function and Modulation. *Front. Mol. Neurosci.* 3:117. https://doi.org/10.3389/fnmol.2010.00117

Tomita, S., H. Adesnik, M. Sekiguchi, W. Zhang, K. Wada, J.R. Howe, R.A. Nicoll, and D.S. Bredt. 2005. Stargazin modulates AMPA receptor gating and trafficking by distinct domains. *Nature.* 435:1052–1058. https://doi.org/10.1038/nature03624

Traynelis, S.F., M. Hartley, and S.F. Heinemann. 1995. Control of proton sensitivity of the NMDA receptor by RNA splicing and polyamines. *Science.* 268:873–876. https://doi.org/10.1126/science.7754371

Traynelis, S.F., L.P. Wollmuth, C.J. McBain, F.S. Menniti, K.M. Vance, K.K. Ogden, K.B. Hansen, H. Yuan, S.J. Myers, and R. Dingledine. 2010.

Glutamate receptor ion channels: structure, regulation, and function. *Pharmacol. Rev.* 62:405–496. https://doi.org/10.1124/pr.109.002451

Tu, Y.C., and C.C. Kuo. 2015. The differential contribution of GluN1 and GluN2 to the gating operation of the NMDA receptor channel. *Pflugers Arch.* 467:1899–1917. https://doi.org/10.1007/s00424-014-1630-z

Tu, Y.C., Y.C. Yang, and C.C. Kuo. 2016. Modulation of NMDA channel gating by Ca^{2+} and Cd^{2+} binding to the external pore mouth. *Sci. Rep.* 6:37029. https://doi.org/10.1038/srep37029

Turetsky, D., E. Garringer, and D.K. Patneau. 2005. Stargazin modulates native AMPA receptor functional properties by two distinct mechanisms. *J. Neurosci.* 25:7438–7448. https://doi.org/10.1523/JNEUROSCI.1108-05.2005

Twomey, E.C., and A.I. Sobolevsky. 2018. Structural Mechanisms of Gating in Ionotropic Glutamate Receptors. *Biochemistry.* 57:267–276. https://doi.org/10.1021/acs.biochem.7b00891

Twomey, E.C., M.V. Yelshanskaya, R.A. Grassucci, J. Frank, and A.I. Sobolevsky. 2017. Channel opening and gating mechanism in AMPA-subtype glutamate receptors. *Nature.* 549:60–65. https://doi.org/10.1038/nature23479

Verdoorn, T.A., N. Burnashev, H. Monyer, P.H. Seeburg, and B. Sakmann. 1991. Structural determinants of ion flow through recombinant glutamate receptor channels. *Science.* 252:1715–1718. https://doi.org/10.1126/science.1710829

Watanabe, J., C. Beck, T. Kuner, L.S. Premkumar, and L.P. Wollmuth. 2002. DRPEER: a motif in the extracellular vestibule conferring high Ca2+ flux rates in NMDA receptor channels. *J. Neurosci.* 22:10209–10216. https://doi.org/10.1523/JNEUROSCI.22-23-10209.2002

Wilding, T.J., and J.E. Huettner. 2019. Cadmium opens GluK2 kainate receptors with cysteine substitutions at the M3 helix bundle crossing. *J. Gen. Physiol.* 151:435–451. https://doi.org/10.1085/jgp.201812234

Wilding, T.J., Y. Zhou, and J.E. Huettner. 2005. Q/R Site Editing Controls Kainate Receptor Inhibition by Membrane Fatty Acids. *J. Neurosci.* 25:9470–9478. https://doi.org/10.1523/JNEUROSCI.2826-05.2005

Wilding, T.J., E. Fulling, Y. Zhou, and J.E. Huettner. 2008. Amino acid substitutions in the pore helix of GluR6 control inhibition by membrane fatty acids. *J. Gen. Physiol.* 132:85–99. https://doi.org/10.1085/jgp.200810009

Wollmuth, L.P. 2019. Prying open a glutamate receptor gate. *J. Gen. Physiol.* 151:396–399. https://doi.org/10.1085/jgp.201812312

Wollmuth, L.P., T. Kuner, C. Jatzke, P.H. Seeburg, N. Heintz, and J. Zuo. 2000. The Lurcher mutation identifies δ 2 as an AMPA/kainate receptor-like channel that is potentiated by $Ca^{(2+)}$. *J. Neurosci.* 20:5973–5980. https://doi.org/10.1523/JNEUROSCI.20-16-05973.2000

Yamada, K.A., and C.M. Tang. 1993. Benzothiadiazides inhibit rapid glutamate receptor desensitization and enhance glutamatergic synaptic currents. *J. Neurosci.* 13:3904–3915. https://doi.org/10.1523/JNEUROSCI.13-09-03904.1993

Yuan, H., K. Erreger, S.M. Dravid, and S.F. Traynelis. 2005. Conserved structural and functional control of N-methyl-D-aspartate receptor gating by transmembrane domain M3. *J. Biol. Chem.* 280:29708–29716. https://doi.org/10.1074/jbc.M414215200

Yuan, H., K.B. Hansen, K.M. Vance, K.K. Ogden, and S.F. Traynelis. 2009. Control of NMDA receptor function by the NR2 subunit amino-terminal domain. *J. Neurosci.* 29:12045–12058. https://doi.org/10.1523/JNEUROSCI.1365-09.2009

Zhang, J.B., S. Chang, P. Xu, M. Miao, H. Wu, Y. Zhang, T. Zhang, H. Wang, J. Zhang, C. Xie, et al. 2018. Structural Basis of the Proton Sensitivity of Human GluN1-GluN2A NMDA Receptors. *Cell Rep.* 25:3582–3590.e4. https://doi.org/10.1016/j.celrep.2018.11.071

Zhou, Y., X.M. Xia, and C.J. Lingle. 2015. Cadmium-cysteine coordination in the BK inner pore region and its structural and functional implications. *Proc. Natl. Acad. Sci. USA.* 112:5237–5242. https://doi.org/10.1073/pnas.1500953112

Zuo, J., P.L. De Jager, K.A. Takahashi, W. Jiang, D.J. Linden, and N. Heintz. 1997. Neurodegeneration in Lurcher mice caused by mutation in delta2 glutamate receptor gene. *Nature.* 388:769–773. https://doi.org/10.1038/42009
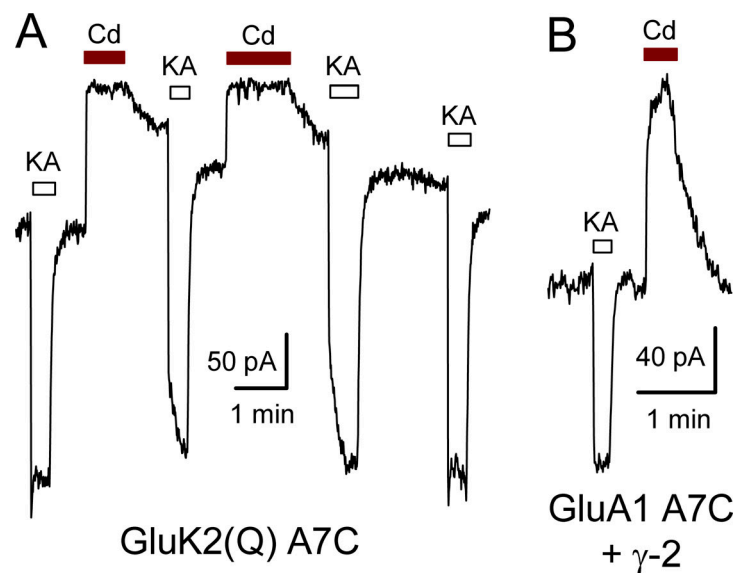
Supplemental material

Figure S1.   **Cd reduces holding current in A7C mutant GluK2(Q) or GluA1. (A)** Whole-cell current during exposure to 10 µM kainate (open bars) or 100 µM Cd (red bars) in an HEK293 cell transfected with GluK2(Q) A7C. Note the slow recovery from Cd inhibition in the absence and presence of kainate. **(B)** Current during exposure to 100 µM kainate or 50 µM Cd in a cell cotransfected with GluA1 A7C and γ-2 TARP.
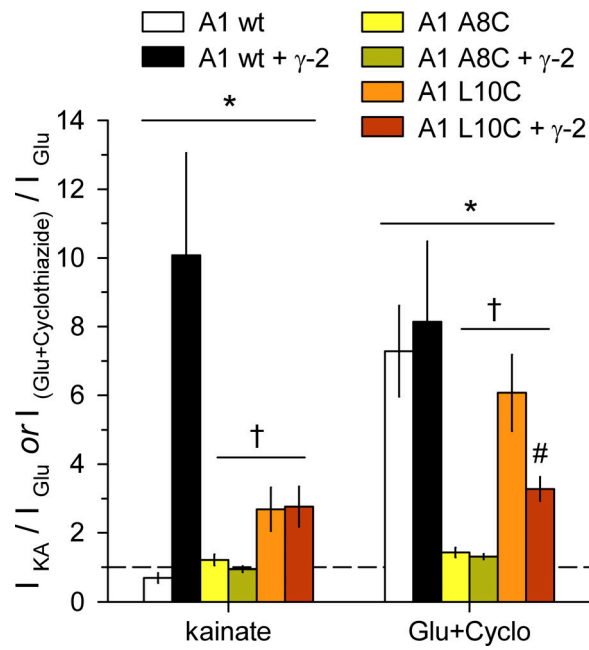
Figure S2. **Activation by kainate or glutamate plus cyclothiazide.** Summary plot of current (mean ± SEM, 5–14 cells per construct) evoked by 100 µM kainate or by 1 mM glutamate plus 30 µM cyclothiazide in HEK293 cells transfected with WT, A8C, or L10C mutant GluA1, alone or cotransfected with γ-2 TARP. *, both A8C and L10C mutants were significantly different from WT; †, A8C was significantly different from L10C; #, L10C with γ-2 TARP was significantly different from L10C alone two-way ANOVA with post hoc Student–Newman-Keuls test).
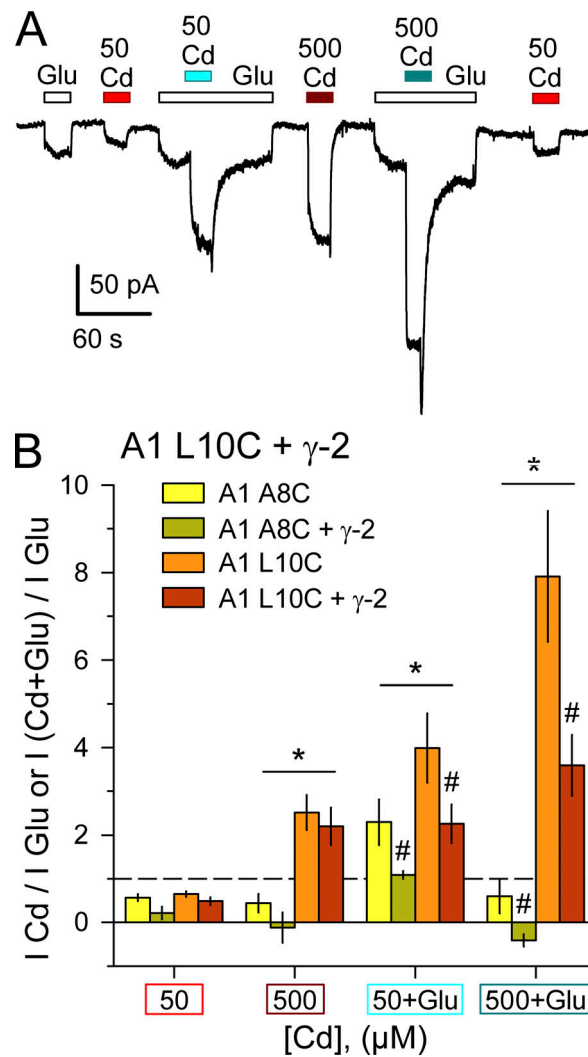
Figure S3. **Activation by Cd compared with glutamate. (A)** Whole-cell current evoked by 1 mM glutamate (open bars), 50 µM or 500 µM Cd alone (red bars), or together with glutamate (cyan bars) in a cell cotransfected with GluA1 L10C and γ-2 TARP. **(B)** Summary plot of current (mean ± SEM, 5–12 cells per construct) evoked by Cd alone or Cd plus glutamate as a fraction of current evoked by glutamate alone. * denotes significant difference between A8C and L10C. # indicates significant difference with γ-2 TARP coexpression (two-way ANOVA with post hoc Student–Newman-Keuls test).

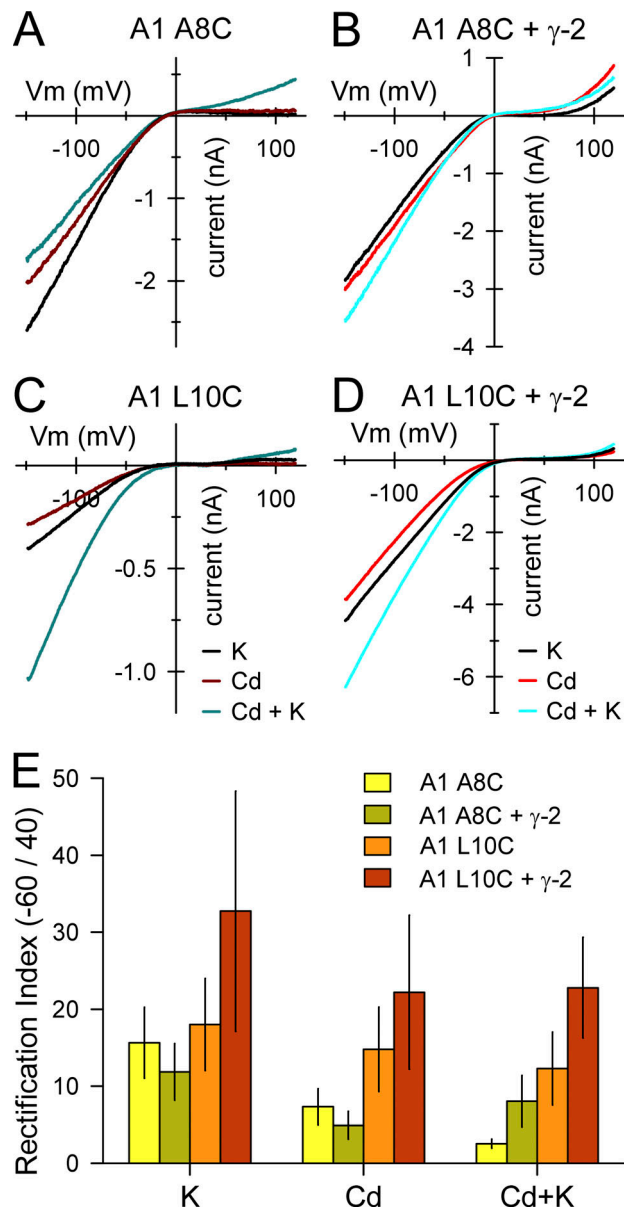Figure S4. **Inward rectification of GluA1 A8C and L10C. (A–D)** Currents evoked by 100 µM kainate, 400 µM Cd alone or together with kainate during voltage ramps from −150 to +120 mV. **(E)** Rectification index (mean ± SEM ratio of current at −60 mV to +40 mV; 5–11 cells per construct) for currents evoke by kainate, Cd alone, or together with kainate. Higher index values indicate stronger rectification. Values for GluA1 L10C + γ-2 TARP were significantly greater than for GluA1 A8C expressed alone or together with γ-2 (2-way ANOVA with post hoc Student–Newman–Keuls test).

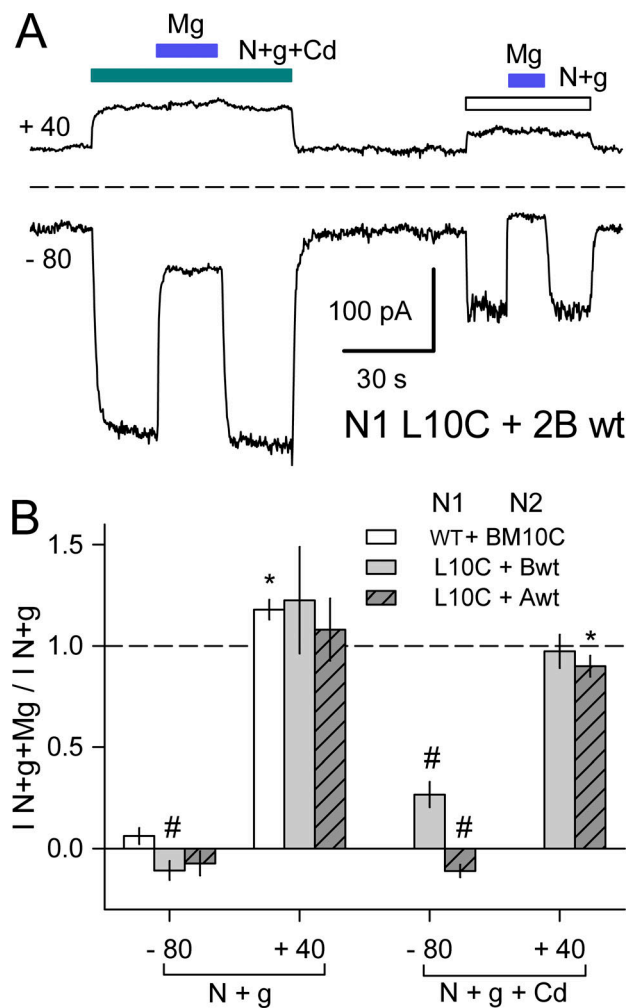Figure S5. **Mg block of NMDA receptors with N1 L10C or N2B M10C mutations. (A)** Whole-cell currents evoked by 10 µM NMDA + glycine alone (open bar) or together with 500 µM Cd (cyan bar) in a cell cotransfected with N1 L10C and N2B WT. Blue bars indicate coapplication of 1 mM Mg. Traces depict current averaged over 2.5-ms intervals while holding at −80 mV and during 50-ms steps to +40 mV delivered at 5 Hz. **(B)** Summary plot of currents (mean ± SEM, four to six cells per construct) evoked at −80 and +40 mV in the presence of 1 mM Mg as a fraction of current in Mg-free solution for NMDA + glycine alone or together with Cd. * denotes significant difference from $I_{N+g+Mg}/I_{N+g} = 1$ (t test). # denotes significant difference from $I_{N+g+Mg}/I_{N+g} = 0$ (t test).
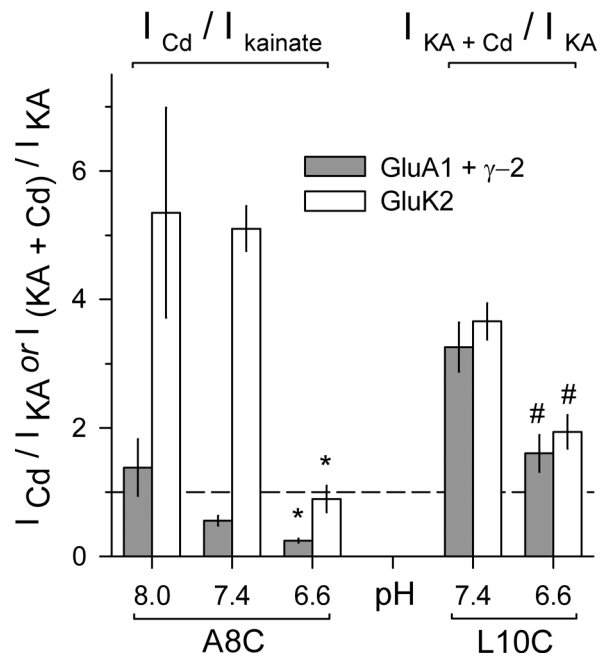
Figure S6. **Protons inhibit Cd activation of Cys substituted AMPA and kainate receptors.** Current (mean ± SEM, 5–39 cells per condition) evoked by Cd alone or together with kainate as a fraction of current evoked by kainate alone. Homomeric receptors with A8C (left) or L10C (right) substitutions were tested at different external pH levels in HEK293 cells transfected with mutant GluK2 (open bars) or cotransfected with mutant GluA1 and stargazin (γ-2 TARP; gray bars). * denotes significant difference from pH 8.0 and 7.4 (ANOVA on ranks with post hoc Dunn's test). # denotes significant difference from pH 7.4 (Mann–Whitney rank sum test).